Technical Report

Title: ***Laboratory Geomechanical Strength Testing of DGR-2 to DGR-6 Core***

Document ID: **TR-09-07**

Authors: **B. Gorski, D. Rodgers and B. Conlon**
CANMET Mining and Mineral Sciences Laboratories, Natural Resources Canada

Revision: **0**

Date: **April 7, 2011**

DGR Site Characterization Document
Geofirma Engineering Project 08-200

Geofirma Engineering Ltd

Geofirma Engineering DGR Site Characterization Document		
Title:	Laboratory Geomechanical Strength Testing of DGR-2 to DGR-6 Core	
Document ID:	TR-09-07	
Revision Number:	0	Date: April 7, 2011
Authors:	B. Gorski, D. Rodgers and B. Conlon CANMET Mining and Mineral Sciences Laboratories Natural Resources Canada	
Technical Review:	Kenneth Raven, Dougal McCreath (Laurentian University); Tom Lam (NWMO)	
QA Review:	John Avis	
Approved by:	Kenneth Raven	

Document Revision History		
Revision	Effective Date	Description of Changes
0	April 7, 2011	Initial Release

TABLE OF CONTENTS

LIST OF APPENDICES

1 Introduction

Geofirma Engineering Ltd. (formerly Intera Engineering Ltd.) has been contracted by the Nuclear Waste Management Organization (NWMO) to implement the Geoscientific Site Characterization Plan (GSCP) for the Bruce nuclear site located on Lake Huron, Ontario. The purpose of this site characterization work is to assess the suitability of the Bruce nuclear site to construct a Deep Geologic Repository (DGR) to store low-level and intermediate-level radioactive waste. The GSCP is described by Intera Engineering Ltd. (2006, 2008).

This Technical Report summarizes the results of laboratory geomechanical strength testing of core obtained from two deep inclined bedrock boreholes (DGR-5 and DGR-6) as part of Phase 2B of the GSCP, as well as supplementary testing of core previously collected during drilling of boreholes DGR-2, DGR-3 and DGR-4. Core samples from DGR boreholes are identified by borehole number and depth along the borehole in metres (e.g., DGR4-730.55). For vertical boreholes DGR-1 to DGR-4, sample depths are reported in metres below ground surface (mBGS). For inclined boreholes DGR-5 and DGR-6, sample depths are reported as metres length below ground surface (mLBGS). Conversion of formation depths in mLBGS to mBGS for DGR-5 and DGR-6 is given in TR-09-11 (Geofirma Engineering Ltd., 2011a). For DGR-6 core samples collected below a depth of 516.33 mLBGS, the core depths listed in this Technical Report are corrected for depth errors reported by the driller as described in TR-09-01 (Geofirma Engineering Ltd., 2011b).

Natural Resources Canada (NRCan) through the CANMET Mining and Mineral Sciences Laboratories (CANMET-MMSL) was contracted by Geofirma to provide laboratory geomechanical services. The objective of this contract was to determine the mechanical properties of shale, limestone, sandstone and dolostone rock core originating from boreholes DGR-2 to DGR-6. Uniaxial compression and direct shear tests comprised the bulk of the testing program. Triaxial compression tests were also conducted including acoustic emission and velocity measurements. This report describes the test apparatus and procedures and presents the results of the testing program.

Work described in this Technical Report (TR) was completed in accordance with Intera Test Plan TP-09-07 – Geomechanical Lab Testing of DGR-5 & DGR-6 Core (Intera Engineering Ltd., 2009a), prepared following the general requirements of the DGR Project Quality Plan (Intera Engineering Ltd., 2009b).

2 Standard Operating Procedures

The test program was carried out at the CANMET-MMSL's Rock Mechanics test facility located in Bells Corners. The Rock Mechanics test facility is managed by the Ground Control Program. The test facility is an ISO 17025 (International Standards Organization) accredited testing laboratory. Standard Operating Procedures (SOPs) that form part of the facility's accredited test procedures were selected for this project. The Standard Operating Procedures used for this test program were:

SOP-T 2100 Specimen Preparation, Standardization and Dimensional Tolerance Verification,
SOP-T 2103 Compressional P-Wave Velocity Test,
SOP-T 2112 Uniaxial Compressive Strength Test with Servo Computer Control Press,
SOP-T 2113 Uniaxial Elastic Moduli and Poisson's Ratio Test with Servo Computer Control Press,
SOP-T 2114 Triaxial Compressive Strength Test with Servo Computer Control Press,
SOP-T 2115 Triaxial Elastic Moduli and Poisson's Ratio Test with Servo Computer Control Press, and
SOP-T 2098 Direct Shear Test with Constant Normal Load.

3 Specimens

The procedure for the preparation of a cylindrical specimen conforms to the ASTM D4543 standard (ASTM, 2008a) and CANMET-MMSL SOP-T 2100. The wet specimens were jacketed with heat-shrink tubing prior to sample preparation, to minimize the loss or gain of water. The end surfaces of specimens were ground flat to within 0.025 mm, parallel to each other to within 0.025 mm, and perpendicular to the longitudinal axis of the specimen to within 0.25 degrees as determined using a gauge plate and dial gauge.

Specimen lengths were determined to the nearest 0.025 mm by averaging the length measured at four points 90 degrees to each other. Specimen diameters were measured to the nearest 0.025 mm by averaging three measurements taken at the upper, middle and lower sections of the specimens. The average diameter was used for calculating the cross-sectional area. The volumes of the specimens were calculated from the average length and diameter measurements. The weights of the specimens were determined to the nearest 0.01 g and the densities of the specimens were computed to the nearest 0.001 Mg/m^3. The borehole, depth, dimensions, bulk density, and geologic formation of uniaxial and triaxial specimens, are listed in Table A-1.

4 Test Apparatus and Procedure

4.1 Zero Pressure Velocity Tests

Zero pressure P-wave and S-wave velocities were measured for all the uniaxial and triaxial specimens prior to testing. The testing apparatus comprised a pulse generator, power amplifier, pulsing and sensing heads (transmitter and receiver) and oscilloscope. The P-wave and S-wave velocities were measured in accordance with SOP-T2103, and ASTM standard D2845, (ASTM, 2008b).

4.2 Uniaxial and Triaxial Compression Strength Tests

Compressive strength tests were conducted in a computer controlled, servo-hydraulic compression machine, consisting of a 2.22 MN rated load cell, triaxial cell, load frame, hydraulic power supply, digital controller and test software. Three linear variable differential transformers (LVDTs) were arrayed around the specimen at 120 degree intervals for the measurement of axial deformations. A circumferential extensometer was used to measure specimen circumferential deformation.

The test specimens were loaded in stress control to imminent failure in accordance with ASTM standard D7012, (ASTM, 2007) and ISRM (1981). Data were scanned every second and stored digitally in engineering units. Time, axial load, confinement pressure, axial strain and diametric strain were recorded during each test. After testing, the specimens were photographed.

4.3 Acoustic Emission (AE) Tests

Acoustic emission tests were incorporated into 13 of the 21 uniaxial compression tests. The highlighted specimen depths in the tables in Appendix A were not integrated with AE measurements. The AE system consisted of 12 transducer channels, 16 bit, 10 MHz, 40 dB preamplification, 60 dB gain, high and low pass filters and source location software.

Two outer arrays of 3 piezoelectric transducers each were attached to the surface of the uniaxial specimens. Arrays for uniaxial specimens were located in ⅓ the length of the specimens. The transducers were spaced 120 degrees from each other for each array. The bottom array 1 consisted of transducers 1, 2 and 3 and the upper array 2 consisted of transducers 4, 5 and 6. The transducers were numbered clockwise looking down the specimen. Specimen references to top, bottom and down refer to the specimen orientation as retrieved from the borehole. Transducer 1 was orientated over the black line scribed on the specimen by Geofirma personnel. Transducer 4 on array 2 was rotated 60 degrees clockwise away from transducer 1 on array 1.

Acoustic emissions were recorded before, during and after each uniaxial compressive strength test. Time, counts, magnitudes and other data were recorded for each event. The reader is referred to the research paper by Durrheim and Labrie (2004) where the acoustic system is explained in detail.

4.4 Direct Shear Strength Tests

The procedure for the direct shear test conformed to the Standard Operating Test Procedure SOP-T 2098, ASTM Standard D5607 (ASTM, 2008c) and ISRM (1981). The direct shear test machine comprised a shear box, base plate, steel table with two columns and an adjustable crossbar above the table, hydraulic control system, hydraulic ram, spherical seat, electric motor, two load cells, three linear variable differential transformers (LVDTs) and a personal computer. The shear box consisted of two halves of a split box made of cast steel. The lower box was free to move on a roller system along four steel rails that are bolted to the base plate. The lower box was pushed forward and pulled backward by means of a screw jack, equipped with a load cell and driven by a variable speed electric motor. The upper box was stationary in the lateral direction, but was allowed to move in the vertical direction. The reader is referred to the research paper by Lau (2002) where the shear test apparatus is explained in detail.

The specimen was encapsulated in the upper box first. The specimen was then locked in a vise when positioned in the box to ensure that the interface lay in a horizontal position and was 3 to 5 mm above the mold surface. Hydrostone was used as the encapsulating material. The upper box with the specimen set in the hydrostone was then weighed. The upper box was then placed on top of the lower box and the specimen was encapsulated in the lower box. The normal load cell and spherical seat were placed between the upper shear box and the hydraulic ram under the adjustable crossbar. One LVDT was mounted in a horizontal position at the end of the lower shear box and two LVDTs were mounted in a vertical position on top of the upper box for the measurement of shear and normal displacements.

The direct shear test was controlled by computer software. A predetermined normal load was first applied on the sample by means of the hydraulic ram and the hydraulic control system. The normal stiffness was then determined for DGR-5 specimens only. The weight of the normal load system (load cell, spherical seat and the upper box with specimen set in hydrostone) was used in determining the normal load. The shear test was performed by sliding the lower box under the stationary upper box at a shear displacement rate of approximately 0.38 mm/min to a maximum stroke of 10 mm. The normal and shear loads were measured with load cells, and the normal and shear displacements were measured with LVDTs. During testing, analog signals from the load cells and LVDTs were scanned every second. The signals were converted to engineering units and stored in the computer. The computer also provided real time stress-displacement plots throughout the test for monitoring purposes. Photographs of the sheared surfaces were taken. A carpenter’s profilometer was used to transfer the fracture surfaces at ¼ diameter locations.

5 Analysis of Data

5.1 Zero Pressure Velocity Tests

The P-wave (compressive and S-wave (shear)) velocities were determined by dividing the specimen length by the wave travel time through the specimen. The dynamic properties were then calculated using the following equations:

Dynamic Young’s Modulus

$$E_d = \frac{\rho V_s^2 \left(3V_p^2 - 4V_s^2\right)}{V_p^2 - V_s^2} \tag{1}$$

where: E_d = dynamic Young’s modulus
V_s = shear wave velocity

V_p = compressive wave velocity
ρ = density

Dynamic Shear Modulus

$$G_d = \rho V_s^2 \quad (2)$$

where: G_d = dynamic shear modulus
V_s = shear wave velocity
ρ = density

Poisson's Ratio (based on velocity data)

$$\nu_d = \frac{V_p^2 - 2V_s^2}{2\left(V_p^2 - V_s^2\right)} \quad (3)$$

where: ν_d = Poisson's Ratio
V_s = shear wave velocity
V_p = compressive wave velocity

The velocity measurements and calculated dynamic properties are contained in Table A-2.

5.2 Uniaxial and Triaxial Compression Strength Tests

Data obtained from the compression tests included the confining pressure (σ_3), axial stress (σ_1), the axial strain (ε_a) and the circumferential strain (ε_c). Strains were calculated using extensometer data. Stress and strain were calculated as follows:

Axial Stress

$$\sigma_1 = \frac{P}{A_0} \quad (4)$$

where: σ_1 = axial stress
P = applied axial load
A_0 = initial specimen cross-sectional area

Axial Strain

$$\varepsilon_a = \frac{\Delta l}{l_0} \quad (5)$$

where: ε_a = axial strain
Δl = change in length of specimen
l_0 = initial length of specimen

Circumferential Strain

$$\varepsilon_c = \frac{\Delta d}{d_0} \quad (6)$$

where: ε_c = circumferential strain
Δd = change in circumference of specimen
d_0 = initial circumference of specimen

Volumetric Strain

$$\varepsilon_v = \varepsilon_a + 2\varepsilon_c \qquad (7)$$

where: ε_v = volumetric strain
ε_a = axial strain
ε_c = circumferential strain

Ultimate uniaxial compressive strength σ_c, triaxial compressive strength σ_1, tangent Young's modulus of elasticity E, (calculated at 0.4 σ_c) and the Poisson's Ratio v, were established in each uniaxial and triaxial compressive test case as per ASTM Standard D7012, (ASTM, 2007) using load cell, extensometer and strain gauge data. These values were calculated as follows:

Ultimate Uniaxial and Triaxial Compressive Strength

$$\sigma_c = \frac{P_c}{A_0} \quad \text{and} \quad \sigma_1 = \frac{P_c}{A_0} \qquad (8)$$

where: σ_c = ultimate uniaxial compressive strength
σ_1 = ultimate triaxial compressive strength
P = axial load at failure
A_0 = initial specimen cross-sectional area

Young's Modulus of Elasticity

$$E = \frac{\sigma_{40}}{\varepsilon_{40}} \qquad (9)$$

where: E = tangent Young's Modulus at 40% of peak strength
σ_{40} = tangent stress at 40% of peak strength
ε_{40} = tangent strain at 40% of peak strength

Poisson's Ratio

$$v = \frac{E_{axial}}{E_{lateral}} \qquad (10)$$

where: v = Poisson's Ratio
E_{axial} = slope of axial stress-strain curve at 40% of peak strength
$E_{lateral}$ = slope of lateral stress-strain curve at 40% of peak strength

The ultimate uniaxial and triaxial compressive strength, peak strain, Young's Modulus and Poisson's Ratio values are contained in Table A-3. Specimen stress-strain curves are contained in Appendices B and D. The graphs display stress-strain data calculated using extensometers. The strain shifts from the origin for the triaxial stress-strain curves are due to the initial application of confinement stress.

Crack damage stress σ_{cd}, is the stress level where the ε_v-ε_a curve reaches a maximum and starts to reverse in direction, indicating dilation due to the formation and growth of unstable cracks. Progressive fracturing failure process starts above σ_{cd} leading to the failure of the rock. Crack damage stress and crack initiation stress levels are contained in Table A-3. Volumetric strain and crack volumetric strain curves are displayed in Appendices B and D. Appendices C and E contains photographs of the failed specimens.

Crack initiation stress σ_{ci}, is the stress level where the σ-ε_a and ε_{dv}-ε_a curves start to deviate from linear elastic behaviour, indicating the development and growth of stable cracks. The crack volumetric strain ε_{dv} is the difference between the volumetric strain ε_v observed in the test and the elastic volumetric strain ε_{ev} calculated by assuming ideal linear elastic behaviour throughout the test. The value of σ_{ci}, was derived from the plot of the ε_{dv}-ε_a curve.

Crack Volumetric Strain

$$\varepsilon_{dv} = \varepsilon_v - \varepsilon_{ev} \qquad (11)$$

where: ε_{dv} = crack volumetric strain
ε_v = volumetric strain
ε_{ev} = elastic volumetric strain

5.3 Acoustic Emission (AE) Tests

Acoustic Emission (AE) tests provided a non-destructive analysis of micro-crack formation, orientations and mechanisms and their effect on the mechanics of a test specimen. Coalescence of micro-cracks into macro-cracks cause major damage to a specimen and eventually leads to failure. AE are sound waves emitted by micro-cracks as they are created or move. Sound waves propagated through the specimen and were recorded continuously during the uniaxial compressive test.

Cumulative counts were recorded from the 6 AE channels during uniaxial testing. AE counts showed the amount of fracturing that occurred in the specimen. The cumulative hits for the six channels were summed and are plotted as hits versus stress on the figures contained in Appendices B and D. The source locations of AE events are shown displayed three-dimensionally (3D), adjacent to the photograph of the actual failed specimen in Appendices C and E. The 3D graph and the photograph are displayed vertically as per the test configuration. AE transducer locations are shown in green and the source locations are shown in red. AE source locations delineated regions of damage. Micro-crack distributions, mapped in 3D through time, describe damage accumulation, crack coalescence and macro-fracture propagation.

5.4 Direct Sheer Strength Tests

Direct shear tests were conducted on specimens comprising intact and non-intact shear surfaces. Specimens were tested at normal stresses between 1.4, 2.0 or 3.0 MPa. Test results in the form of plots of shear stress versus shear displacement, shear stress versus normal stress and normal stress versus averaged normal displacement are presented in Appendix F. Shear plane profiles are contained in Appendix G.

The direct shear test was performed by applying a shear load on the specimen under a constant normal load and measuring the normal and shear displacements. The stress values were calculated by dividing the loads by the nominal areas (initial cross-sectional areas) of the interfaces (Equations 13 and 14). The test procedure made no provision for the measurement of pore pressures. The stress values determined before shearing were expressed in terms of total stress. After shearing, the shear plane provided a drainage path for dissipation of pore pressures, and the stress values were expressed in terms of effective stress.

$$\sigma_n = \frac{P_n}{A} \tag{13}$$

$$\tau = \frac{P_s}{A} \tag{14}$$

where:
σ_n = normal stress
τ = shear stress
P_n = normal load
P_s = shear load
A = nominal area (for inclined borehole ellipse areas)

Strength values measured in the direct shear test included peak shear strength and residual strength. The strength values were measured from the stress-displacement plots obtained from the shear tests (see Appendix F). Due to the scattering of data in those plots, linear fitting was applied to determine normal stiffness. Table A-4 presents the strength values including the normal stiffness parameters obtained from the shear tests.

6 Results and Conclusions

This report has described the apparatus and procedures used to conduct various mechanical and dynamic property tests on rock units originating from sedimentary bedrock underlying the Bruce Nuclear site. According to ASTM guide D5878, (ASTM, 2008d) the Uniaxial Compressive strengths of each rock unit may be categorized as follows:

Kirkfield	medium strong	(25-50 MPa)
Cobourg	strong	(50-100 MPa)
Cambrian	strong	(50-100 MPa)
Coboconk	very strong	(100-250 MPa)
Gull River	very strong	(100-250 MPa)
Collingwood	very strong	(100-250 MPa)

Young's modulus and Poisson's ratio values were consistent with the strength determinations. AE curves of cumulative hits increase and coincide with the stress-strain curve shifts.

Many of the pre-determined open joints were in fact found to be intact during testing. As a consequence some specimens sheared at other locations, some in the casting material and others along shear planes not perpendicular to the normal axis of loading. Some sheared planes ended up gouging into the casting material during shear displacement. Where specimens sheared in casting material the tests were rejected and supplemental tests were performed on end pieces of sufficient length.

7 Data Quality and Use

Data on geomechanical strength properties of DGR-2, DGR-3, DGR-4, DGR-5 and DGR-6 core described in this Technical Report are based on testing conducted in accordance with established and well defined ASTM testing procedures.

The results presented in this Technical Report are suitable for assessing the geomechanical strength properties of bedrock formations intersected by DGR-2 to DGR-6, and the development of descriptive geomechanical models of the Bruce DGR site.

8 Disclaimer

Any determination and/or reference made in this report with respect to any specific commercial product, process or service by trade name, trademark, manufacturer or otherwise shall be considered to be opinion; CANMET-MMSL makes no, and does not intend to make any, representations or implied warranties of merchantability or fitness for a particular purpose nor is it intended to endorse, recommend or favour any specific commercial product, process or service. The views and opinions of authors expressed herein do not necessarily state or reflect those of CANMET-MMSL and may not be used for advertising or product endorsement purposes.

9 References

ASTM, 2008a. Designation D4543: Standard Practices for Preparing Rock Core as Cylindrical Test Specimens and Verifying Conformance to Dimensional and Shape Tolerances, 2008 Annual Book of ASTM Standards, Section 4: Construction, Volume 04.08: Soil and Rock (I), ASTM International, West Conshohocken (PA), pp. 725-730.

ASTM, 2008b. Designation D2845: Standard Test Method for Laboratory Determination of Pulse Velocities and Ultrasonic Constants of Rock, 2008 Annual Book of ASTM Standards, Section 4: Construction, Volume 04.08: Soil and Rock (I), ASTM International, West Conshohocken (PA), pp. 303-308.

ASTM, 2008c. Designation D5607: Standard Test Method for Performing Laboratory Direct Shear Strength Tests of Rock Specimens under Constant Normal Force, 2008 Annual Book of ASTM Standards, Section 4: Construction, Volume 04.08: Soil and Rock (I), ASTM International, West Conshohocken (PA), pp.: 1391-1402.

ASASTM, 2008d. Designation D5878: Standard Guides for Using Rock-Mass Classification Systems for Engineering Purposes, 2007 Annual Book of ASTM Standards, Section 4: Construction, Volume 04.09: Soil and Rock (II), ASTM International, West Conshohocken (PA), pp. 330-359.

ASTM, 2007. Designation D7012: Standard Test Method for Compressive Strength and Elastic Moduli of Intact Rock Core Specimens under Varying States of Stress and Temperatures; 2007 Annual Book of ASTM Standards, Section 4: Construction, Volume 04.09: Soil and Rock (II), ASTM International, West Conshohocken (PA), pp. 1429-1436.

Durrheim, R.J. and D. Labrie, 2007. "Data-Driven Simulation of the Rock Mass response to Mining (Part 1): Laboratory Experimentation using Nepean Sandstone Models", Challenges in Deep and High Stress Mining, Y. Potvin, J. Hadjigeorgiou and D. Stacey, Editors, Australian Centre for Geomechanics (ACG), Chapter 34, pp. 293-304.

ISRM, 1981. Rock Characterization Testing and Monitoring; ISRM, Pergamon Press; London, England, pp. 113-140.

Geofirma Engineering Ltd., 2011a. Technical Report: Bedrock Formations in DGR-1 to DGR-6, TR-09-01, Revision 0, in preparation, Ottawa.

Geofirma Engineering Ltd., 2011b. Technical Report: Drilling, Logging and Sampling of DGR-5 and DGR-6, TR-09-01, Revision 0, April 6, Ottawa.

Intera Engineering Ltd., 2009a. Test Plan for Geomechanical Lab Testing of DGR-6 & DGR-6 Core, TP-09-07, Revision 0, August 5, Ottawa.

Intera Engineering Ltd., 2009b. Project Quality Plan, DGR Site Characterization, Revision 4, August 14, Ottawa.

Intera Engineering Ltd., 2008. Phase 2 Geoscientific Site Characterization Plan, OPG's Deep Geologic Repository for Low and Intermediate Level Waste, Report INTERA 06-219.50-Phase 2 GSCP-R0, OPG 00216-REP-03902-00006-R00, April, Ottawa.

Intera Engineering Ltd., 2006. Geoscientific Site Characterization Plan, OPG's Deep Geologic Repository for Low and Intermediate Level Waste, Report INTERA 05-220-1, OPG 00216-REP-03902-00002-R00, April, Ottawa

Lau, J.S.O., 2002. A laboratory Testing Program to Investigate the Mechanisms Leading to Debonding at Concrete-Rock Interfaces, JSO Lau Consulting Services Inc., Ottawa, Ontario: 51p.

APPENDIX A

Data and Calculation Tables

Table A-1. Formations, dimensions and densities of UCS and TCS specimens

Depth (m)	Formation	Length (mm)	Diameter (mm)	Mass (g)	Density (Mg/m³)
DGR2-678.88	Cobourg	169.63	75.66	2034.22	2.67
DGR3-693.82	Cobourg	169.89	75.39	2029.13	2.68
DGR4-682.22	Cobourg	166.02	75.38	1971.94	2.66
DGR4-727.95	Kirkfield	169.46	75.48	2009.20	2.65
DGR4-730.55	Kirkfield	162.76	75.25	1921.15	2.65
DGR4-771.71	Coboconk	168.42	75.87	2057.11	2.70
DGR4-773.38	Coboconk	169.72	75.95	2079.25	2.70
DGR4-808.56	Gull River	167.28	75.64	2034.49	2.71
DGR4-809.88	Gull River	167.86	75.66	2046.69	2.71
DGR4-856.29	Cambrian	170.42	75.66	1697.62	2.22
DGR4-856.80	Cambrian	166.29	75.63	1710.35	2.29
DGR5-700.65	Collingwood	170.03	76.18	2002.89	2.58
DGR5-702.81	Collingwood	169.71	75.92	2059.01	2.68
DGR5-711.96	Cobourg	162.13	75.88	1968.89	2.69
DGR5-719.38	Cobourg	169.96	75.85	2060.22	2.68
DGR5-731.27	Cobourg	169.91	75.83	2052.15	2.67
DGR5-735.61	Cobourg	166.78	76.14	2032.13	2.68
DGR6-747.99	Cobourg	187.14	82.69	2700.37	2.69
DGR6-755.19	Cobourg	186.63	82.71	2696.43	2.69
DGR6-770.07	Cobourg	187.06	82.68	2709.11	2.70
DGR6-773.82	Cobourg	187.39	82.60	2700.67	2.69

NB: Bolded samples were not subject to AE testing.

Table A-2. Dynamic elastic constants of UCS and TCS specimens

Depth	Length	P-wave time	P-wave velocity	S-wave time	S-wave velocity	E	Shear modulus	Poisson's ratio
(m)	(mm)	(μs)	(km/s)	(μs)	(km/s)	(GPa)	(GPa)	(v)
DGR2-678.88	169.63	32.8	5.17	60.4	2.81	54.32	21.04	0.29
DGR3-693.82	169.89	37.1	4.58	62.5	2.72	48.55	19.77	0.23
DGR4-682.22	166.02	37.2	4.46	67.3	2.47	41.46	16.20	0.28
DGR4-727.95	169.46	57.7	2.94	98.1	1.73	19.54	7.91	0.24
DGR4-730.55	162.76	83.0	1.96	171.0	0.95	6.47	2.40	0.35
DGR4-771.71	168.42	28.7	5.87	50.8	3.32	75.17	29.70	0.27
DGR4-773.38	169.72	28.0	6.06	51.3	3.31	76.23	29.60	0.29
DGR4-808.56	167.28	30.5	5.48	52.9	3.16	67.72	27.07	0.25
DGR4-809.88	167.86	31.2	5.38	54.3	3.09	64.97	25.91	0.25
DGR4-856.29	170.42	64.8	2.63	118.0	1.44	11.87	4.62	0.28
DGR4-856.80	166.29	52.7	3.16	87.0	1.91	20.25	8.36	0.21
DGR5-700.65	170.03	40.1	4.24	69.9	2.43	38.37	15.29	0.25
DGR5-702.81	169.71	30.3	5.60	54.6	3.11	66.16	25.90	0.28
DGR5-711.96	162.13	30.4	5.33	54.0	3.00	61.40	24.21	0.27
DGR5-719.38	169.96	30.8	5.52	55.6	3.06	64.11	25.07	0.28
DGR5-731.27	169.91	37.9	4.48	65.3	2.60	45.12	18.10	0.25
DGR5-735.61	166.78	32.9	5.07	60.9	2.74	51.93	20.07	0.29
DGR6-747.99	187.14	33.6	5.57	60.0	3.12	66.47	26.14	0.27
DGR6-755.19	186.63	33.1	5.64	59.8	3.12	67.01	26.19	0.28
DGR6-770.07	187.06	32.4	5.77	58.6	3.19	70.36	27.49	0.28
DGR6-773.82	187.39	34.6	5.42	61.8	3.03	62.90	24.73	0.27

NB: Bolded samples were not subject to AE testing.

Table A-3 Static elastic constants of UCS and TCS specimens

Depth	UCS or σ_1-σ_3	Transducers					
		Peak strain	E	Poisson's ratio	Crack damage stress	Crack Initiation stress	Comments
(m)	(MPa)	(%)	(GPa)	(ν)	(σ_s=MPa)	(σ_d=MPa)	(Mode)[1]
DGR2-678.88	157.71	0.42	47.44	0.23	151.35	60.98	C
DGR3-693.82	83.56	0.36	36.24	0.37	60.47	31.34	A, C
DGR4-682.22	86.18	0.41	25.66	0.33	70.89	33.99	C
DGR4-727.95	59.25	0.44	22.09	0.13	37.99	23.36	C, BD
DGR4-730.55	50.36	0.69	14.23	0.11	46.42	19.62	C, BD
DGR4-771.71	189.31	0.33	68.43	0.27	---	---	C, BD
DGR4-773.38	186.49	0.32	66.93	0.35	136.61	72.67	C
DGR4-808.56	155.74	0.32	58.01	0.29	140.55	63.86	C
DGR4-809.88	108.82	0.26	54.18	0.24	98.36	44.36	C
DGR4-856.29	59.98	0.46	21.26	0.29	37.79	24.11	D
DGR4-856.80	84.80	0.51	24.23	0.36	51.12	34.99	D, BD
DGR5-700.65	175.04	0.87	28.11	0.29	132.92	66.20	σ_3=24 MPa B, 65º
DGR5-702.81	171.21	0.45	49.31	0.23	---	---	σ_3=8 MPa A, 75º
DGR5-711.96	123.18	0.38	40.77	0.34	99.11	56.52	A, C
DGR5-719.38	121.64	0.35	44.90	0.36	112.0	44.05	A, C
DGR5-731.27	81.99	0.36	31.66	0.31	53.03	31.90	A, C
DGR5-735.61	63.67	0.31	36.74	0.24	50.58	26.26	C
DGR6-747.99	113.83	0.25	53.91	0.29	110.09	42.81	C
DGR6-755.19	133.38	0.28	55.21	0.31	116.99	48.24	C
DGR6-770.07	108.38	0.24	62.22	0.34	82.21	39.27	C
DGR6-773.82	97.75	0.24	50.08	0.39	68.29	39.91	C

Note 1

Failure Modes:

- A axial splitting
- B shear (º)
- C multiple shear
- D Cone
- E Cone and A
- F Cone and B
- G Cone and C

Discontinuities:

- (BG) Bedding – regular layering of units or beds in sedimentary rocks
- (BD) Boundary – surface delineating different rock types or strength
- (CV) Cleavage – closely spaced parallel surfaces of fissility
- (CN) Contact – surface between two non sedimentary rock types
- (GS) Gneissosity – surface parallel to metamorphic lithological layering
- (SC) Schistosity – surface of easy splitting in metamorphic rocks defined by preferred orientation of minerals
- (VN) fracture in rock with less than 3cm of filling

Table A-4 Shear test data for DGR specimens

Depth	Diameter	Borehole Inclination	Normal Stiffness	Peak Shear Data		Residual Stress Data		Comments
(m)	(mm)	(°)	(y=mx+b) Y=MPa X=mm	Peak Shear (MPa)	Normal Stress (MPa)	Residual Shear (MPa)	Normal Stress (MPa)	
DGR2-654.00	75.81	89°		3.15	2.02	0.96	2.02	Sheared outside casting
DGR2-661.36	75.53	89°		8.40	2.03	2.55	2.00	Sheared outside casting
DGR2-665.29	75.92	89°		11.73	2.13	3.03	2.05	Sheared outside casting
DGR3-666.10	75.92	89°		13.43	1.94	No data	No data	Sheared outside casting Shear box binding during residual
DGR4-652.93	75.77	89°		6.75	2.02	2.19	2.02	Sheared partially in casting
DGR4-661.90	75.51	89°		14.01	2.04	2.06	2.03	Sheared partially in casting
DGR5-700.70	75.86	77°	Y=9.28X	7.53	1.42	1.61	1.41	Sheared outside casting on scribe Normal stiffness data
DGR5-705.90	75.71	77°	Y=8.51X	4.02	1.42	1.56	1.41	Sheared outside casting on scribe Normal stiffness data
DGR5-719.65	75.32	77°	Y=8.20X	10.64	3.06	1.56	3.02	Sheared outside casting not on scribe Normal stiffness data
DGR5-725.50	75.78	77°	Y=8.30X	12.39	3.10	No data	No data	Sheared in casting not on scribe Normal stiffness data
DGR5-729.70	75.82	77°	Y=8.49X	7.60	1.42	1.70	1.42	Sheared slightly in casting near scribe Normal stiffness data
DGR5-732.20	75.83	77°	Y=8.75X	4.87	1.44	1.49	1.31	Sheared outside casting on scribe Normal stiffness data
DGR5-739.00	75.82	77°	Y=7.42X	-	-	-	-	Joint opened during casting infilling shear plane with hydrostone Normal stiffness data
DGR5-741.90	75.66	77°	Y=7.16X	3.29	1.35	1.33	1.41	Sheared outside casting on scribe Normal stiffness data

APPENDIX B

Stress-Strain Curves of Uniaxial Tests

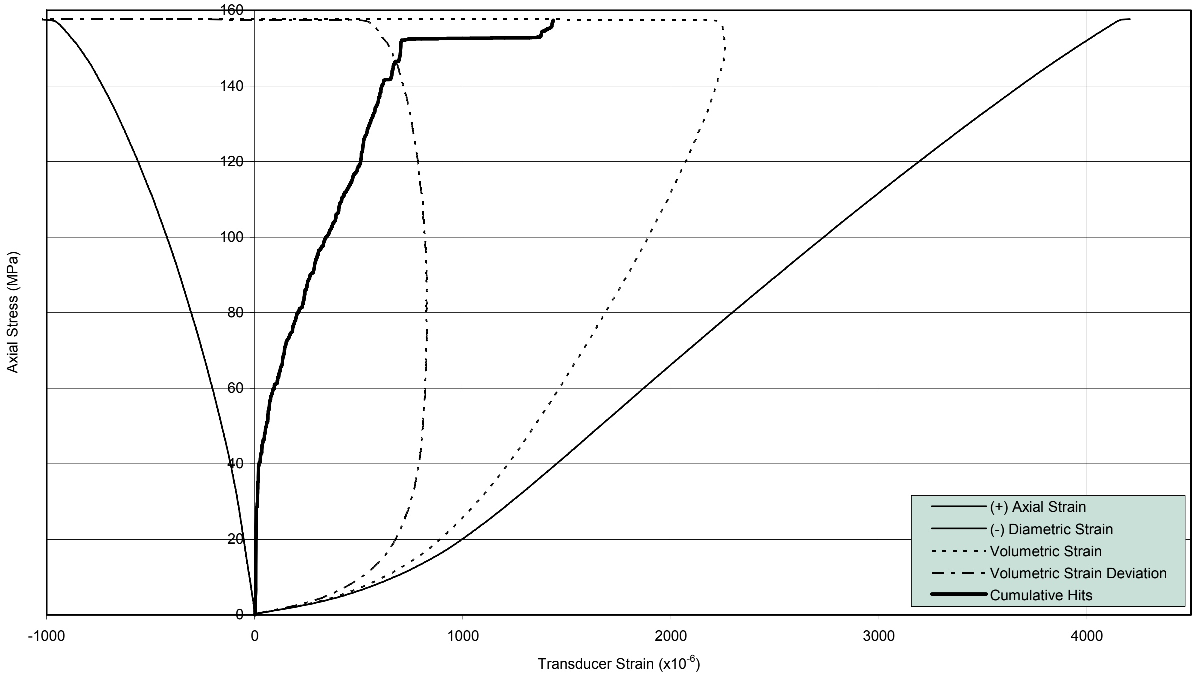

Figure B-1 UCS Specimen DGR-2, 678.88 m

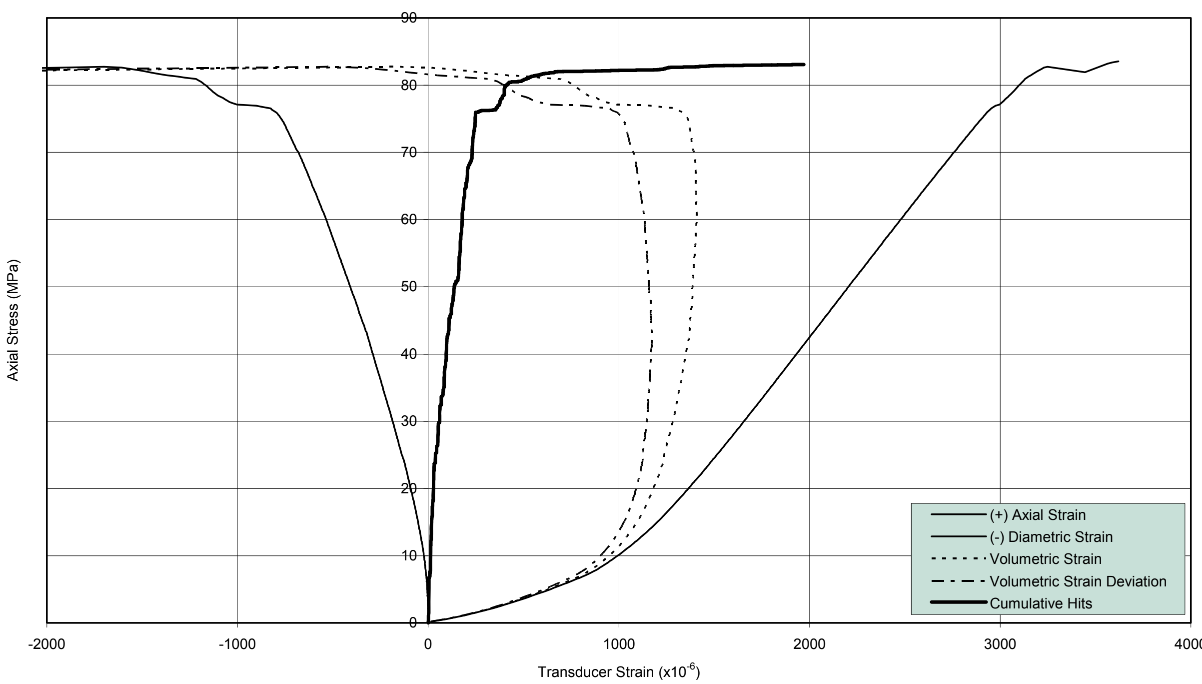

Figure B-2 UCS Specimen DGR-3, 693.82 m

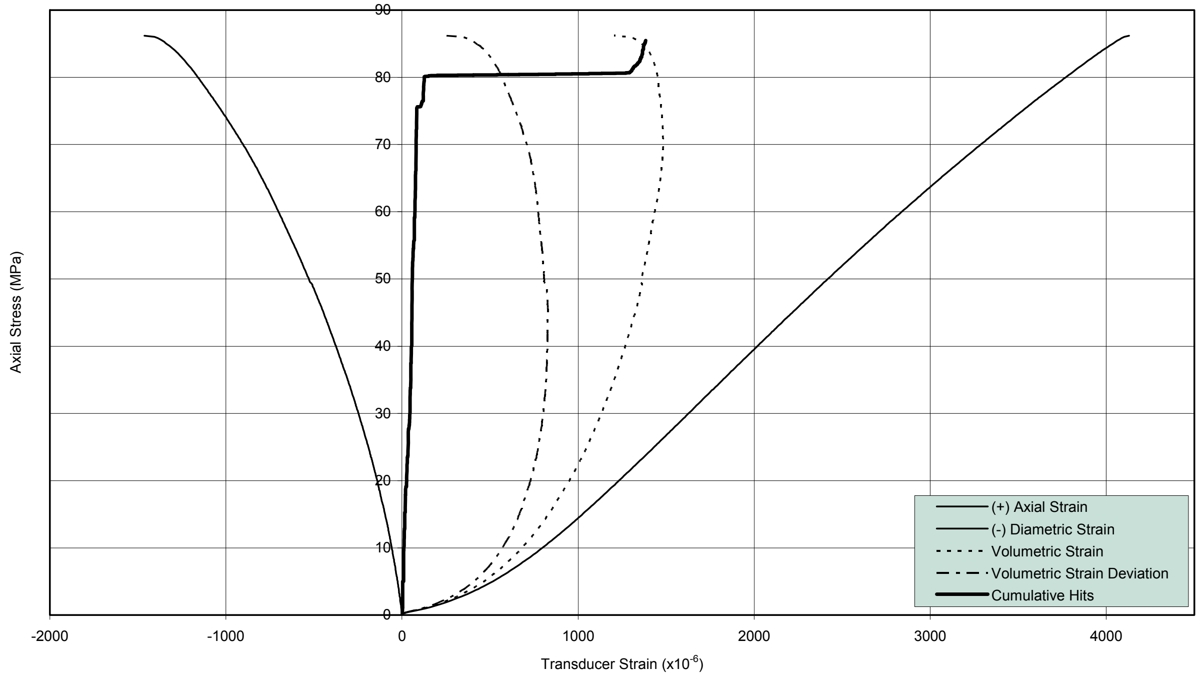

Figure B-3 UCS Specimen DGR-4, 682.22 m

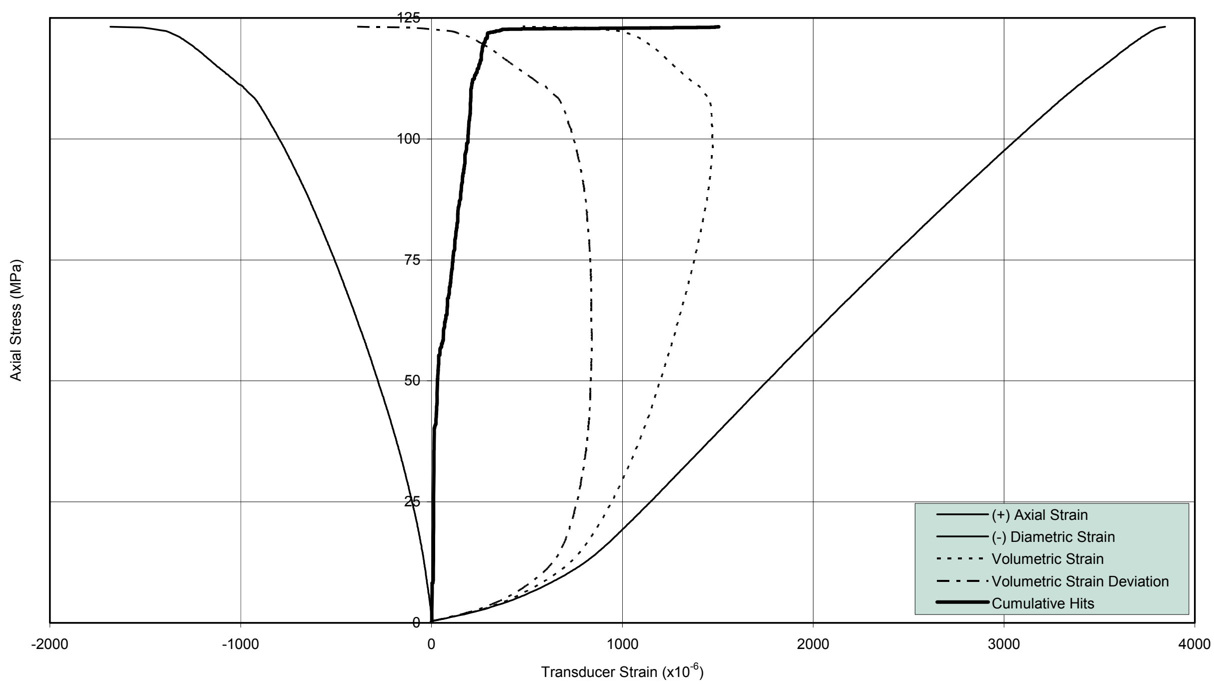

Figure B-4 UCS Specimen DGR-5, 711.96 m

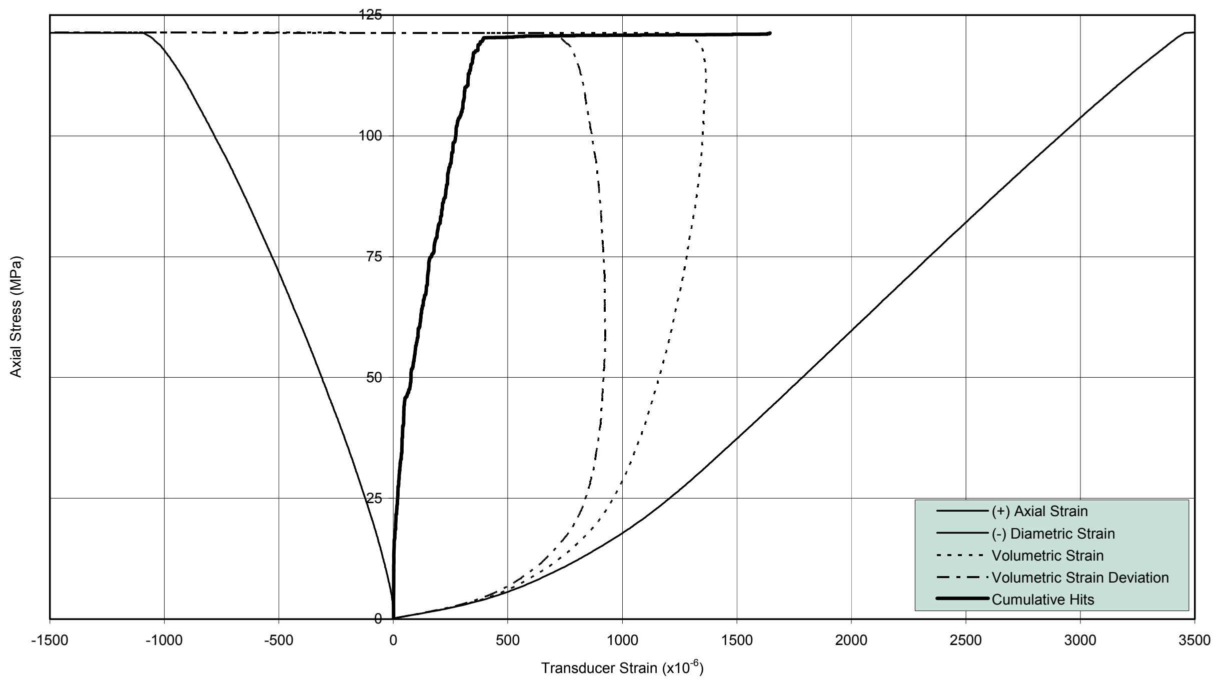

Figure B-5 UCS Specimen DGR-5, 719.38 m

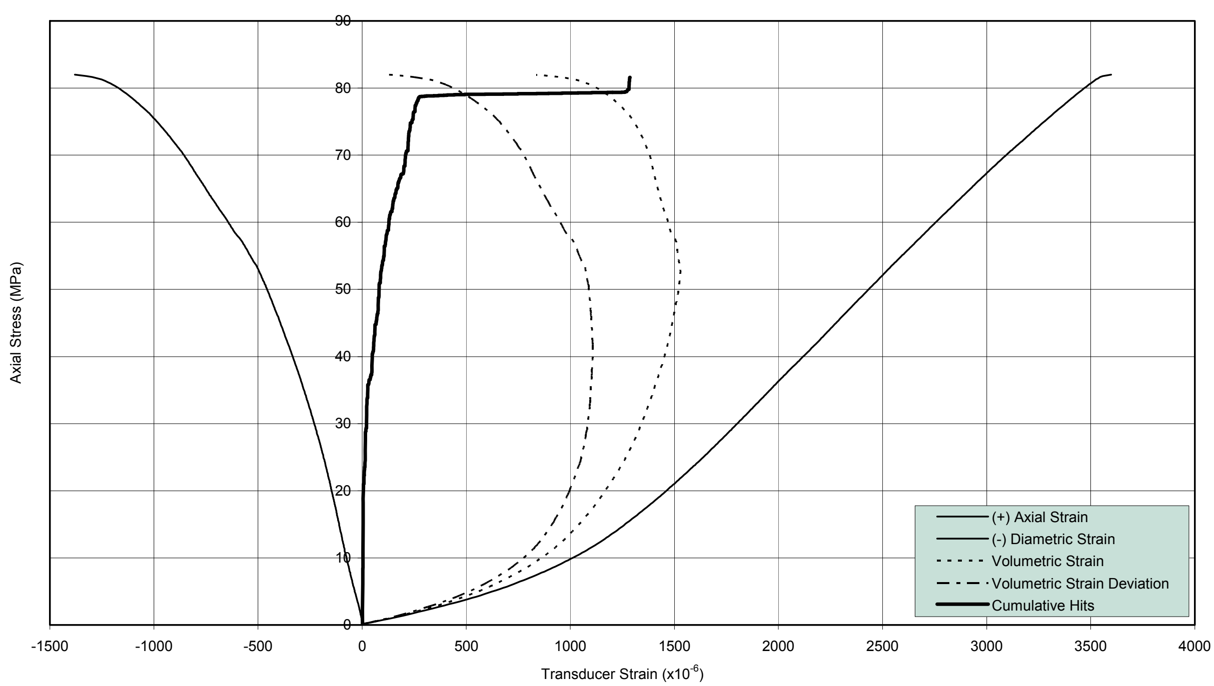

Figure B-6 UCS Specimen DGR-5, 731.27 m

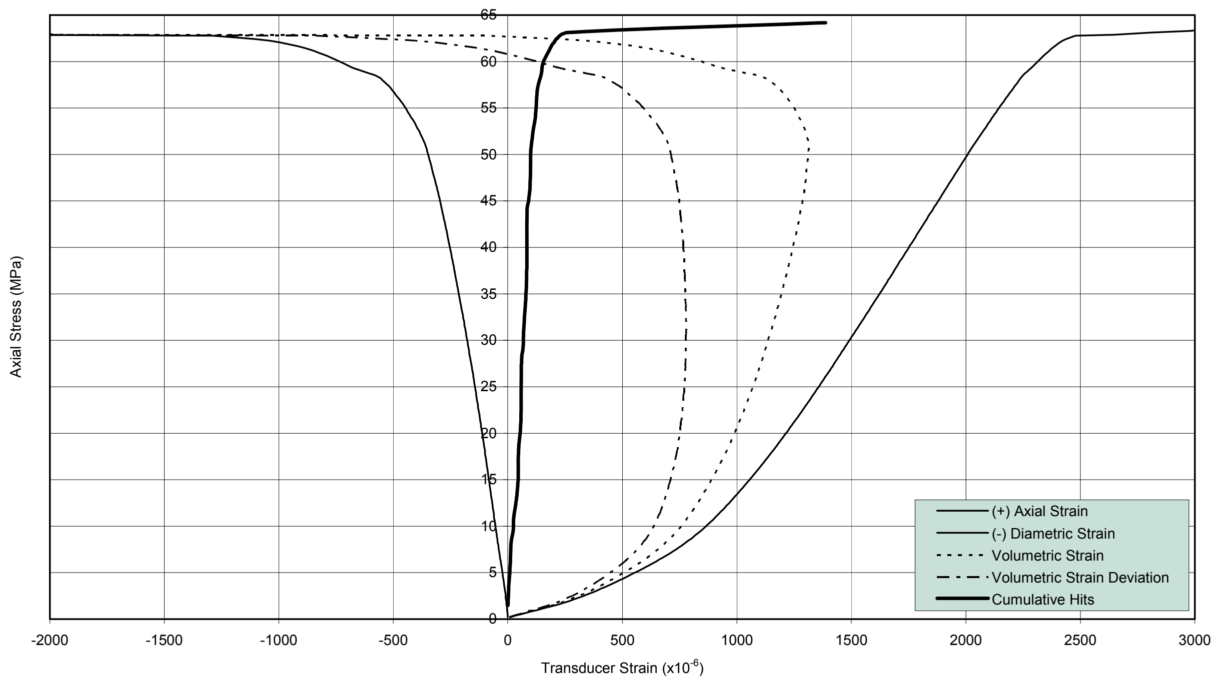

Figure B-7 UCS Specimen DGR-5, 735.61 m

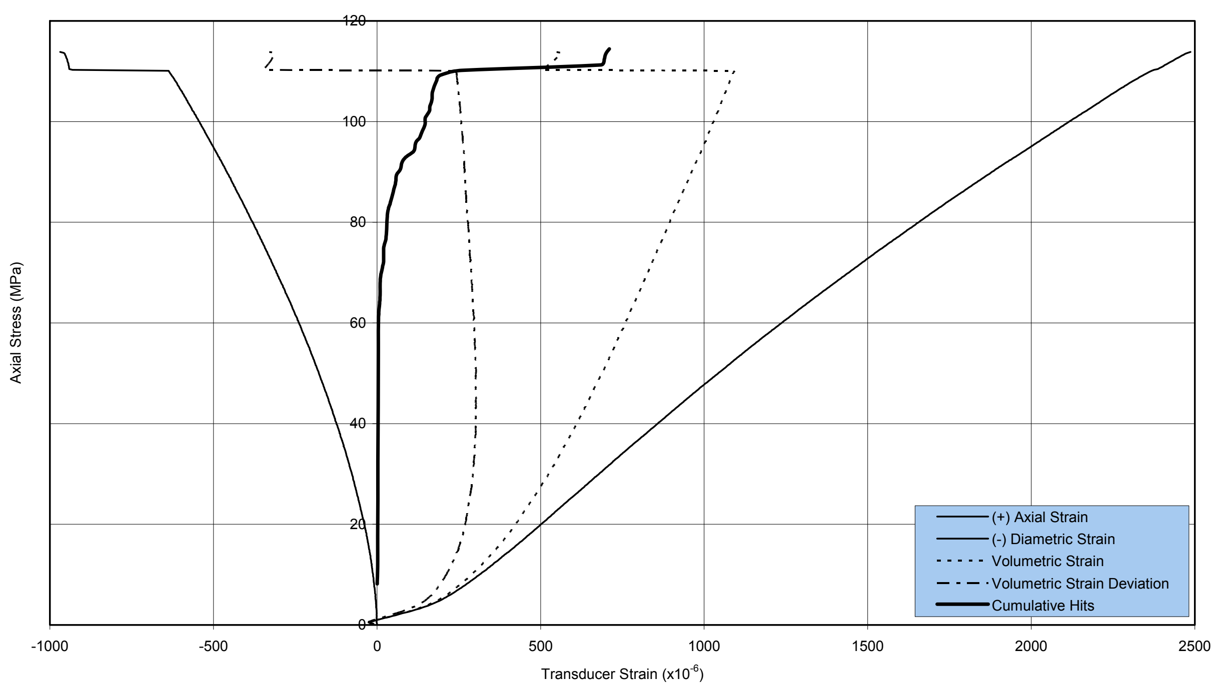

Figure B-8 UCS Specimen DGR-6, 747.99 m

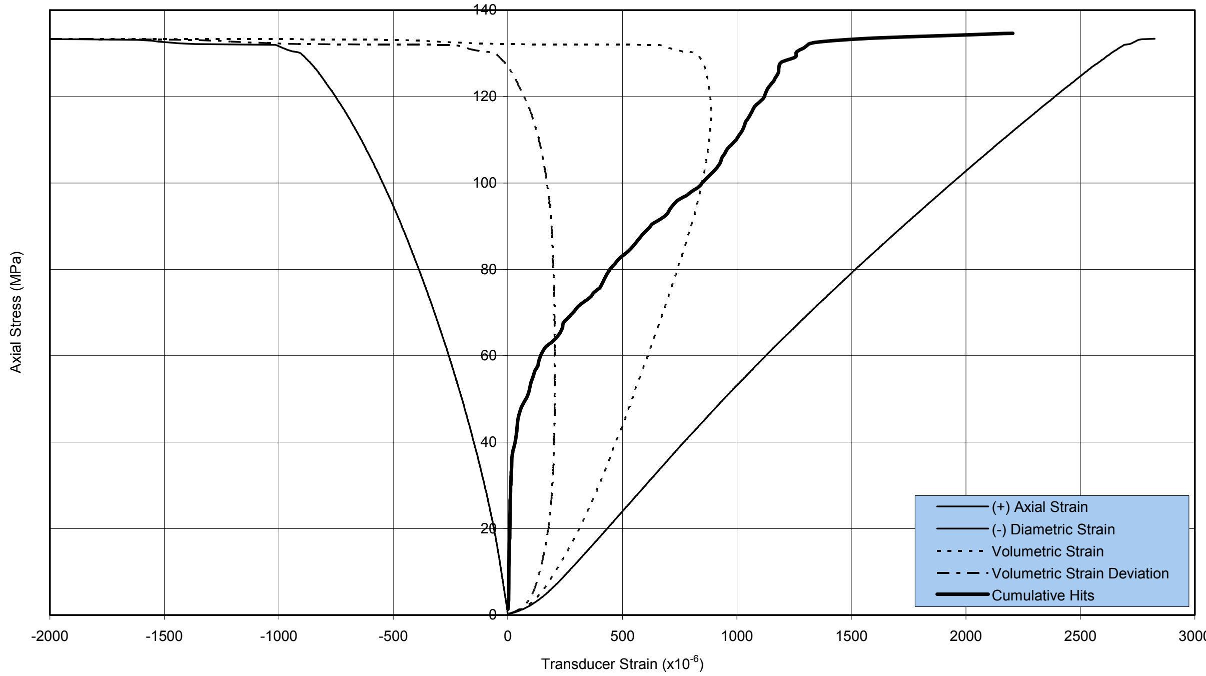

Figure B-9 UCS Specimen DGR-6, 755.19 m

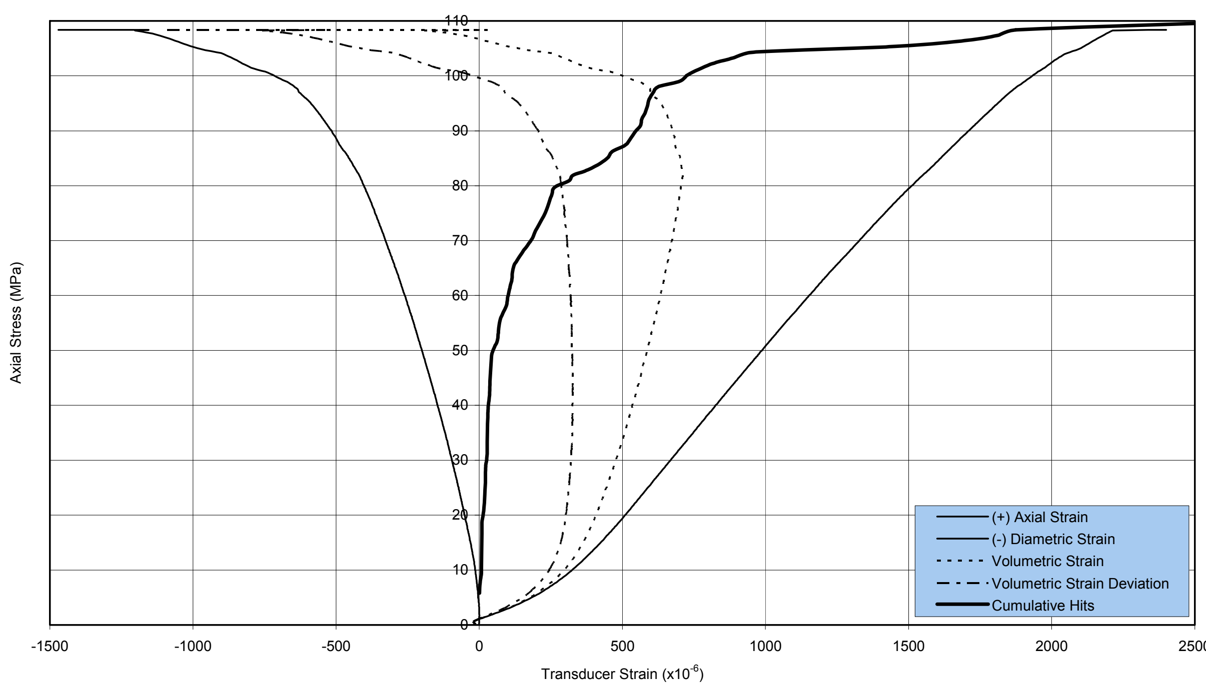

Figure B-10 UCS Specimen DGR-6, 770.07 m

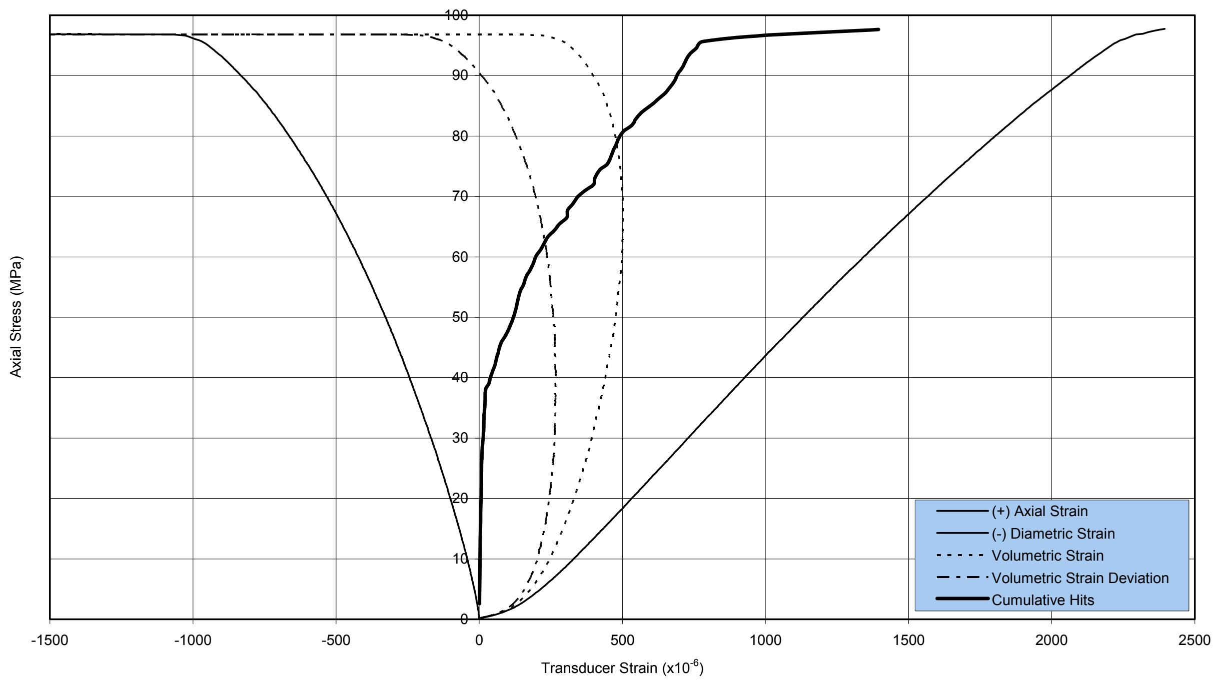

Figure B-11 UCS Specimen DGR-6, 773.82 m

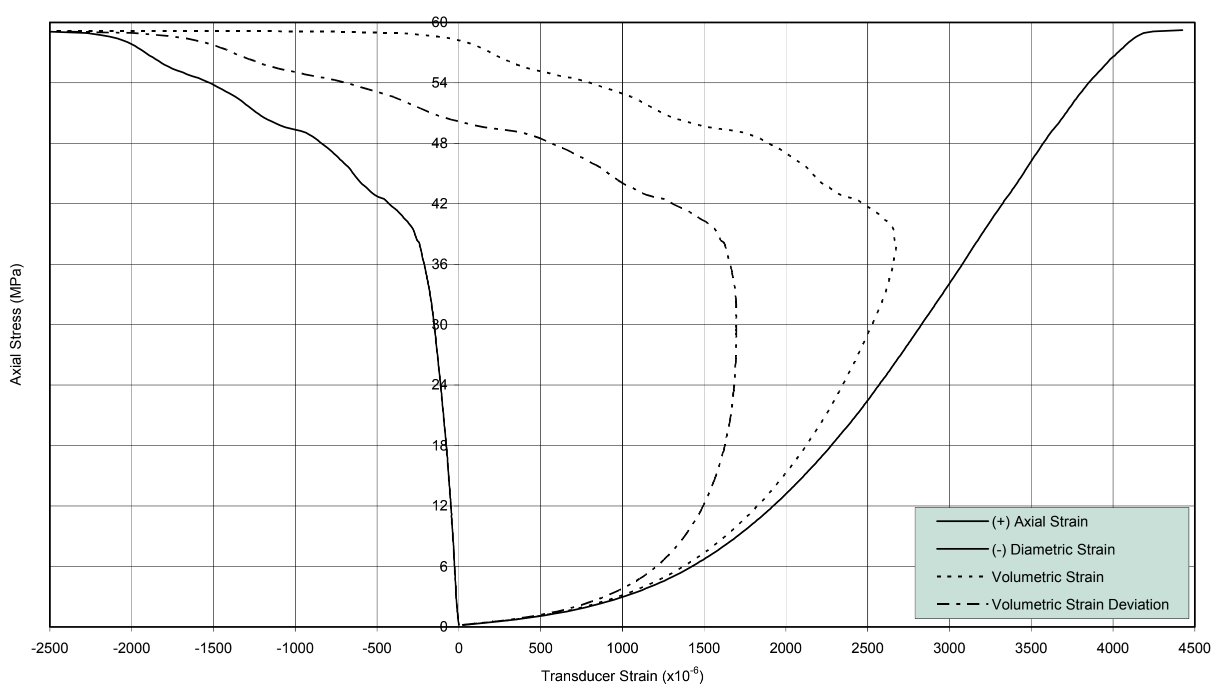

Figure B-12 UCS Specimen DGR-4, 727.95 m

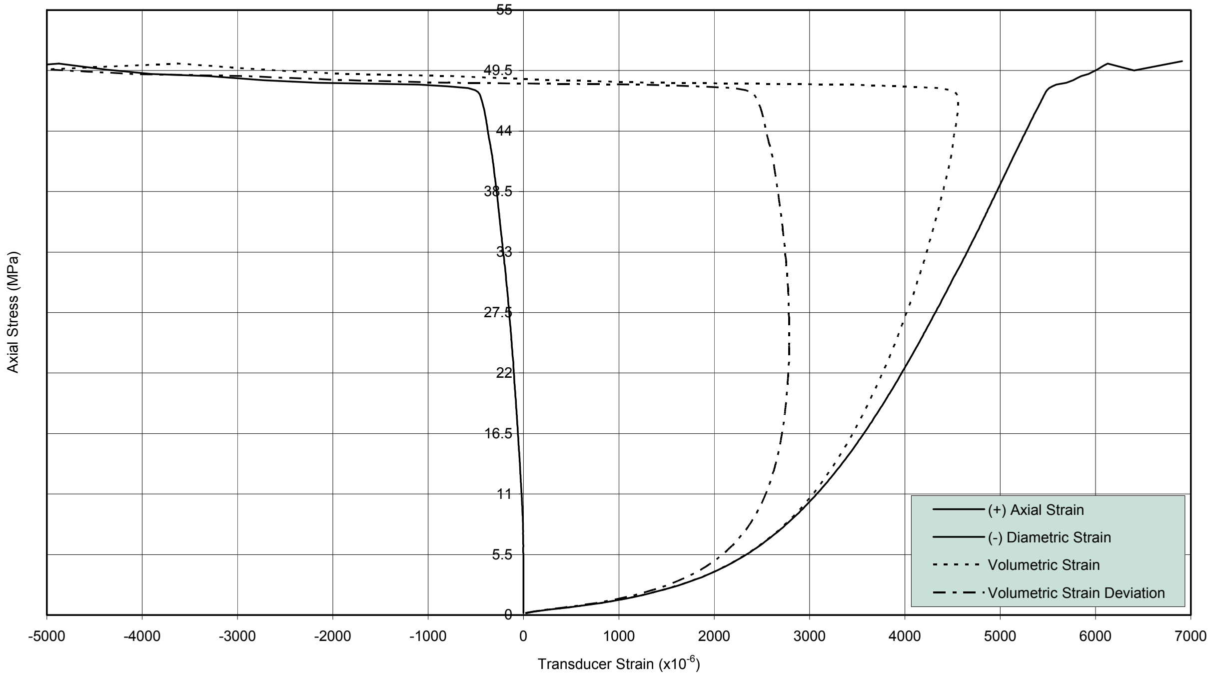

Figure B-13 UCS Specimen DGR-4, 730.55 m

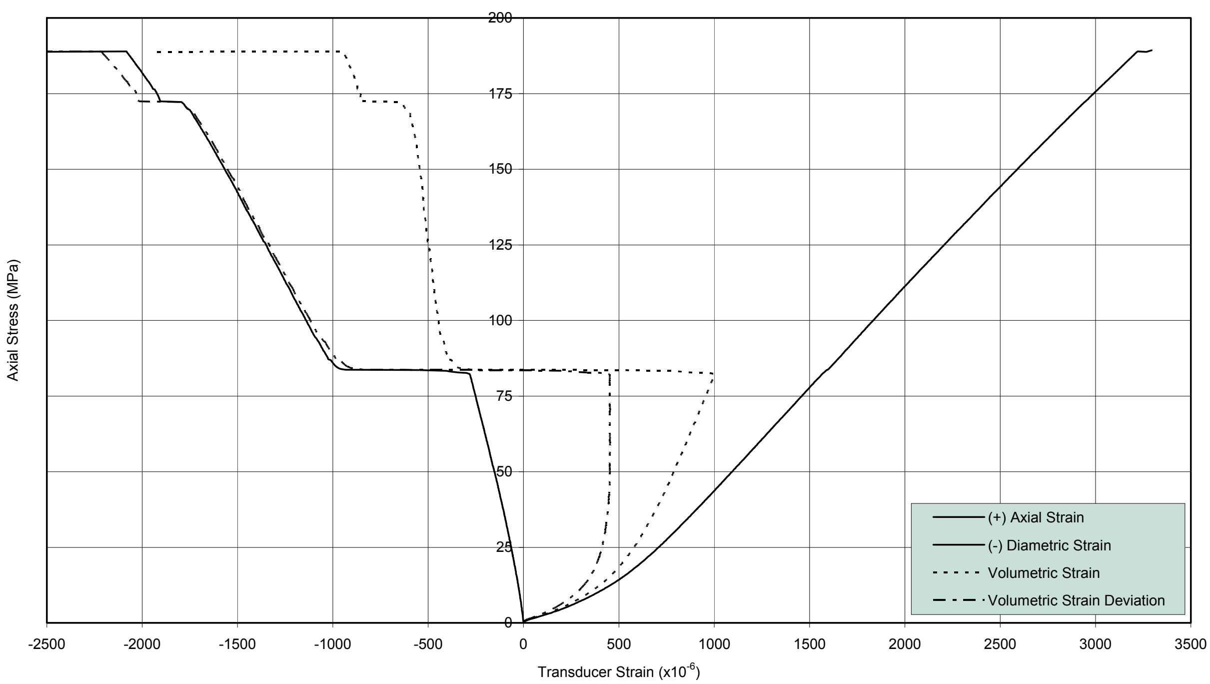

Figure B-14 UCS Specimen DGR-4, 771.71 m

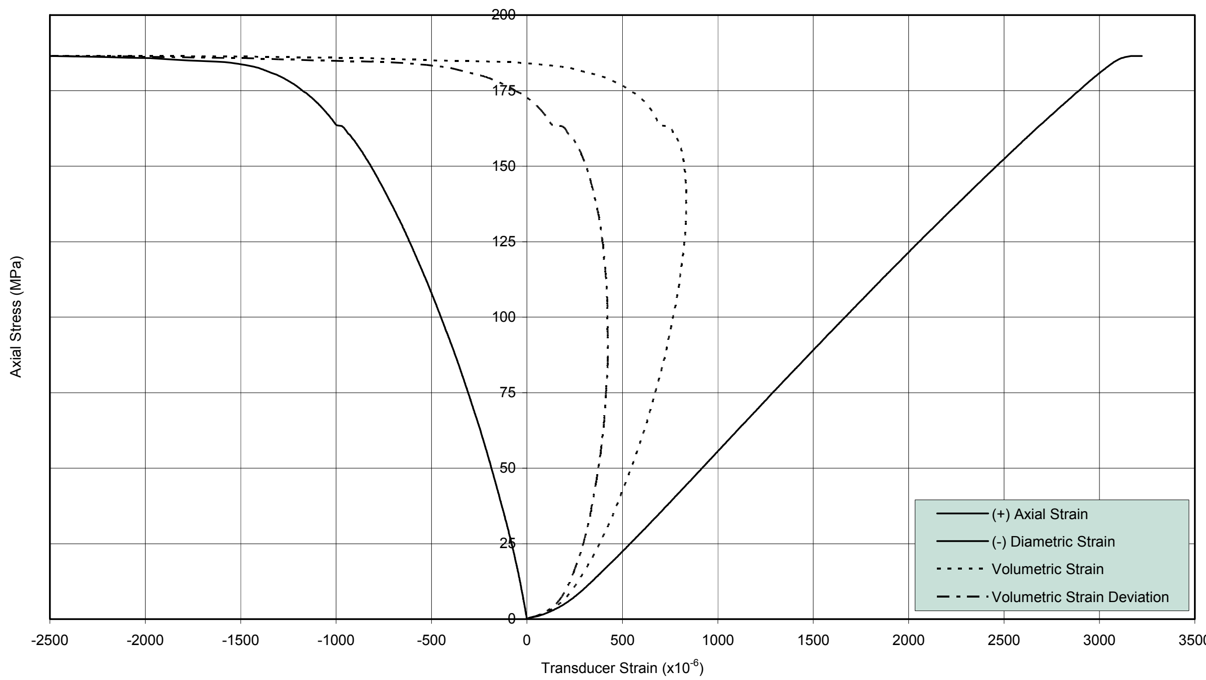

Figure B-15 UCS Specimen DGR-4, 773.38 m

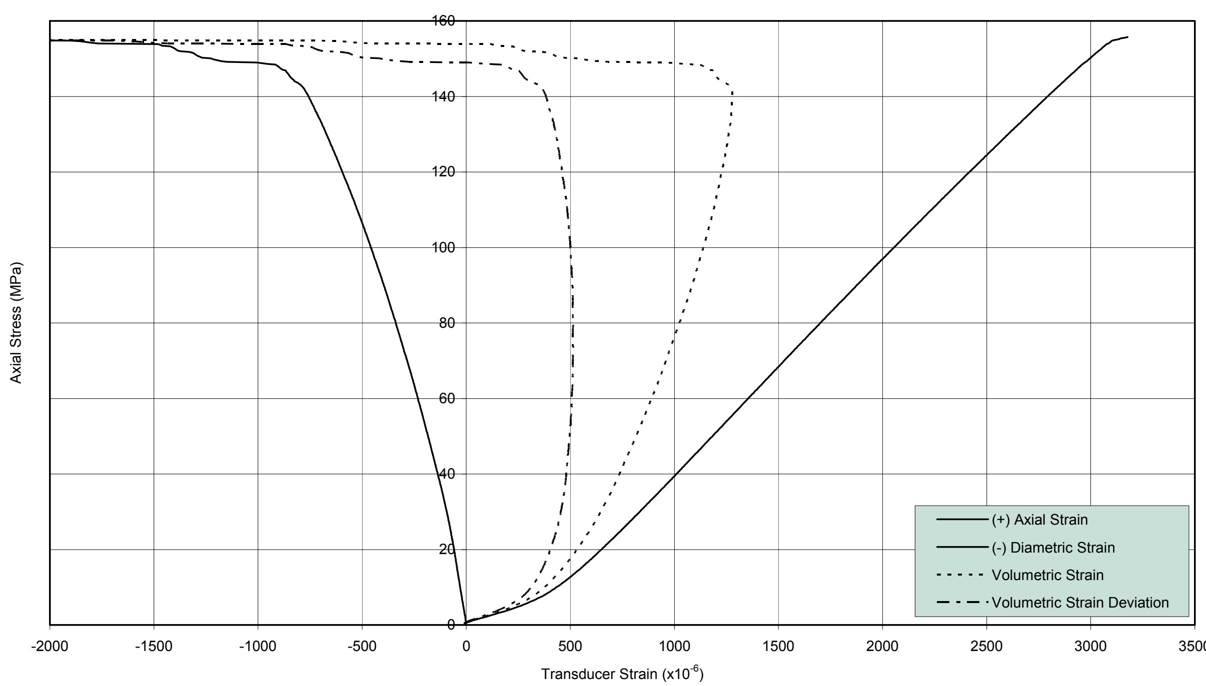

Figure B-16 UCS Specimen DGR-4, 808.56 m

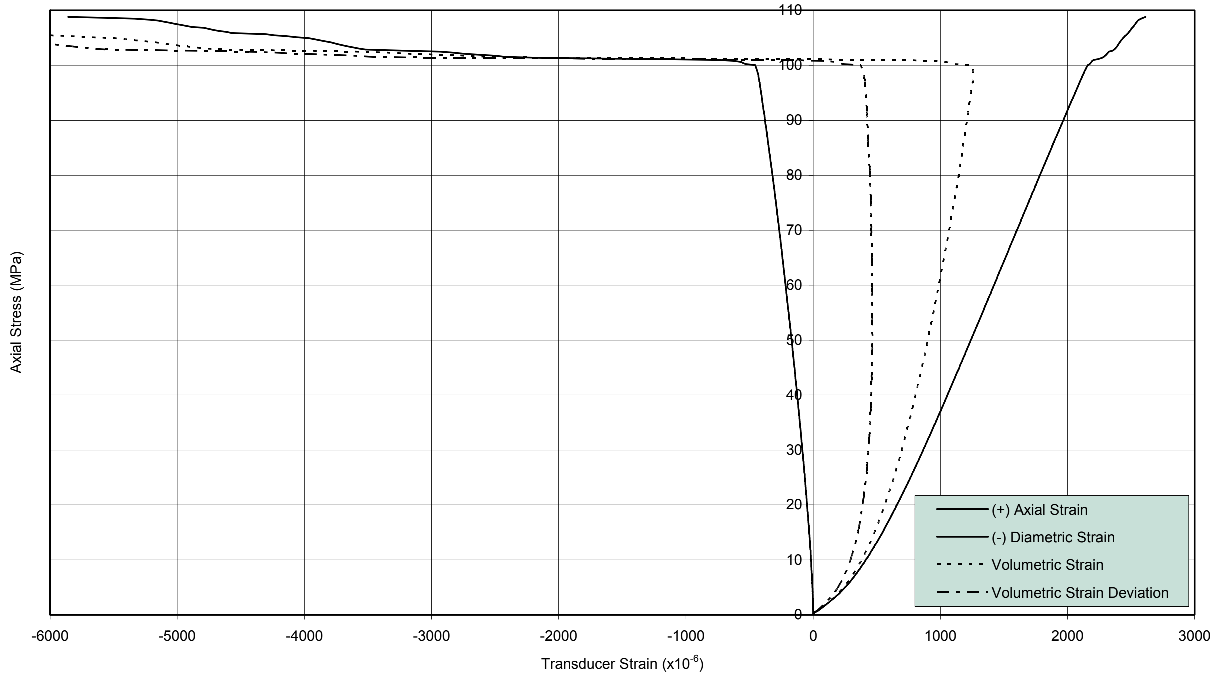

Figure B-17 UCS Specimen DGR-4, 809.88 m

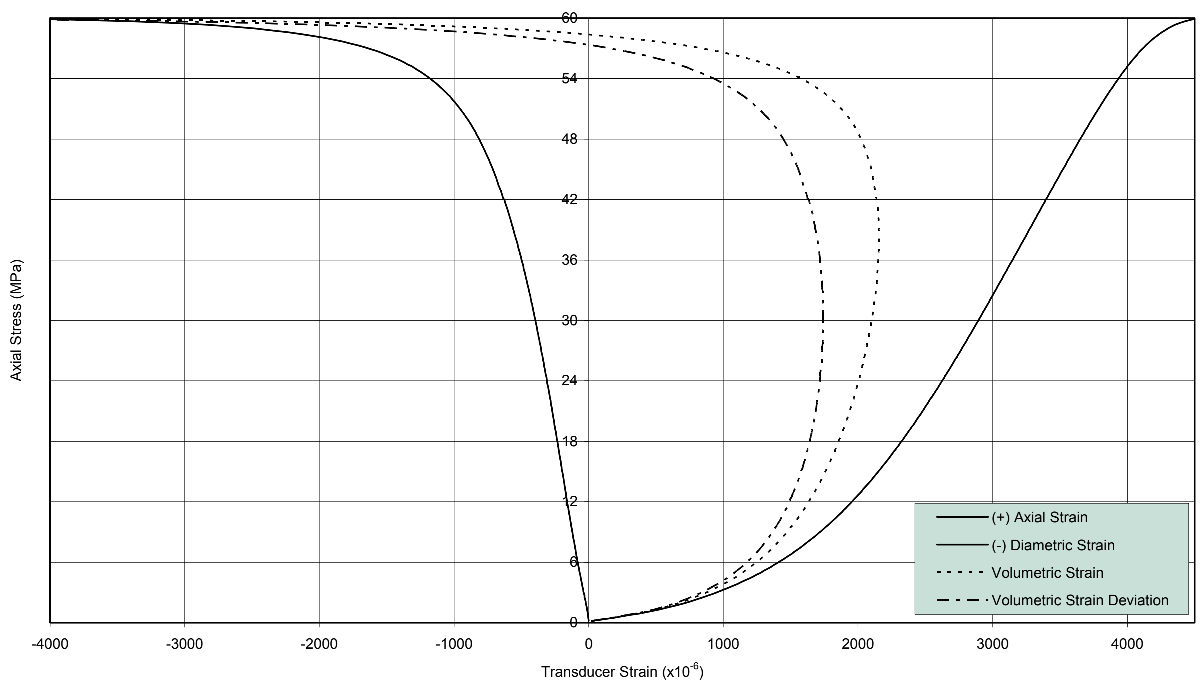

Figure B-18 UCS Specimen DGR-4, 856.29 m

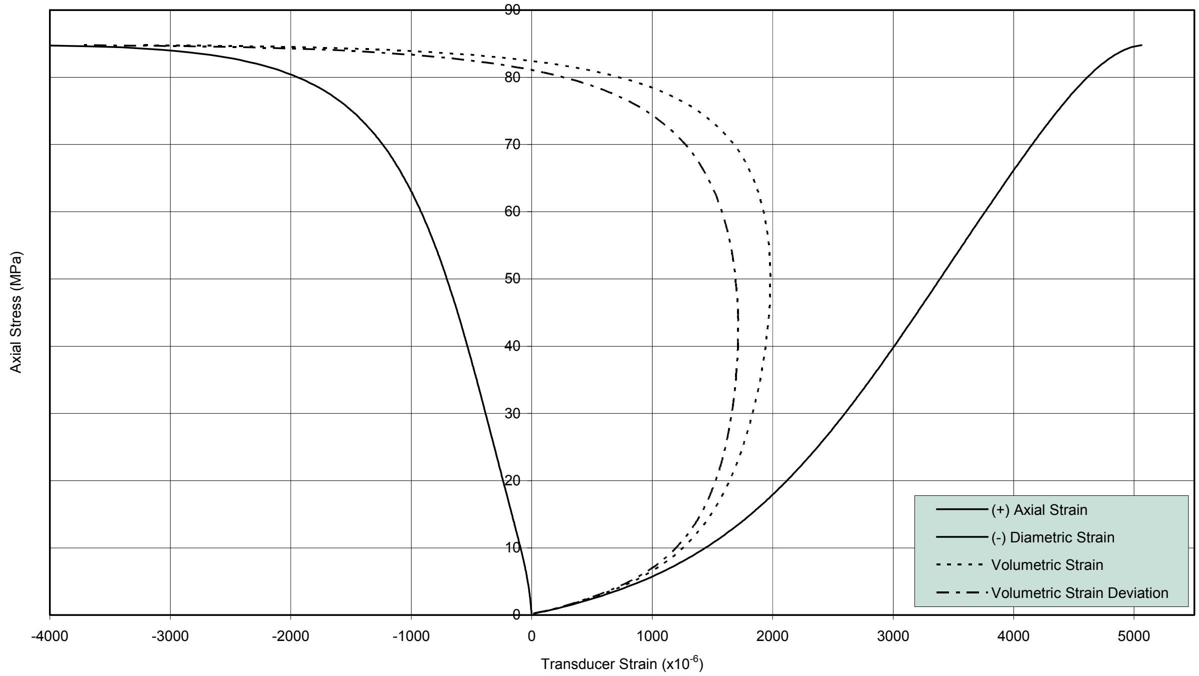

Figure B-19 UCS Specimen DGR-4, 856.80 m

APPENDIX C

Failed Uniaxial Specimens and AE Source Locations

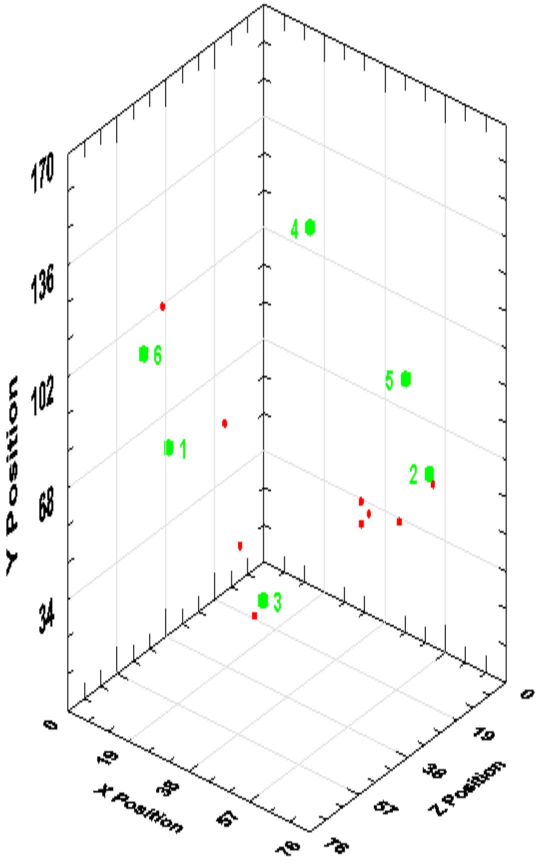

Figure C-1 UCS Specimen DGR2 678.88 m

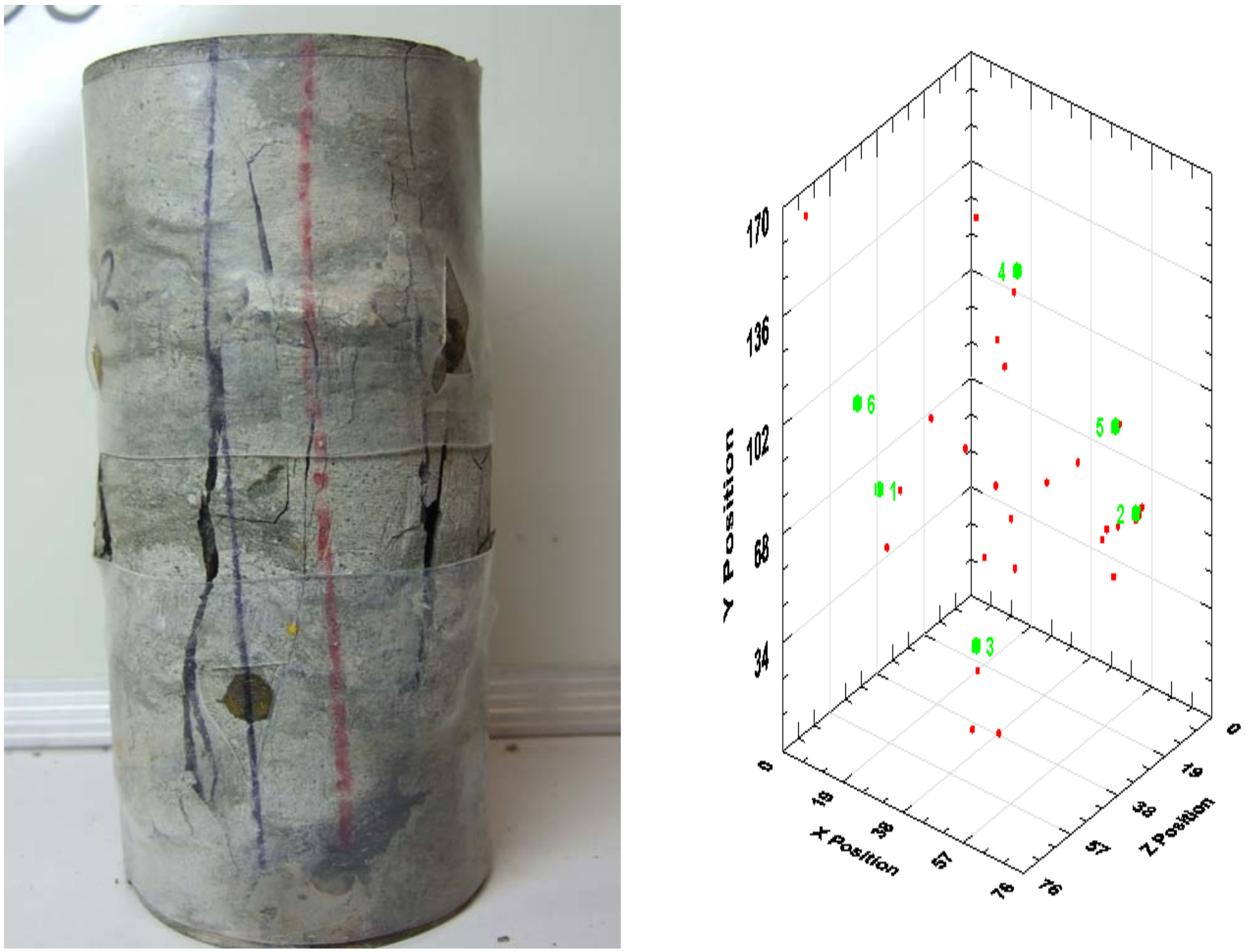

Figure C-2 UCS Specimen DGR3 693.82 m

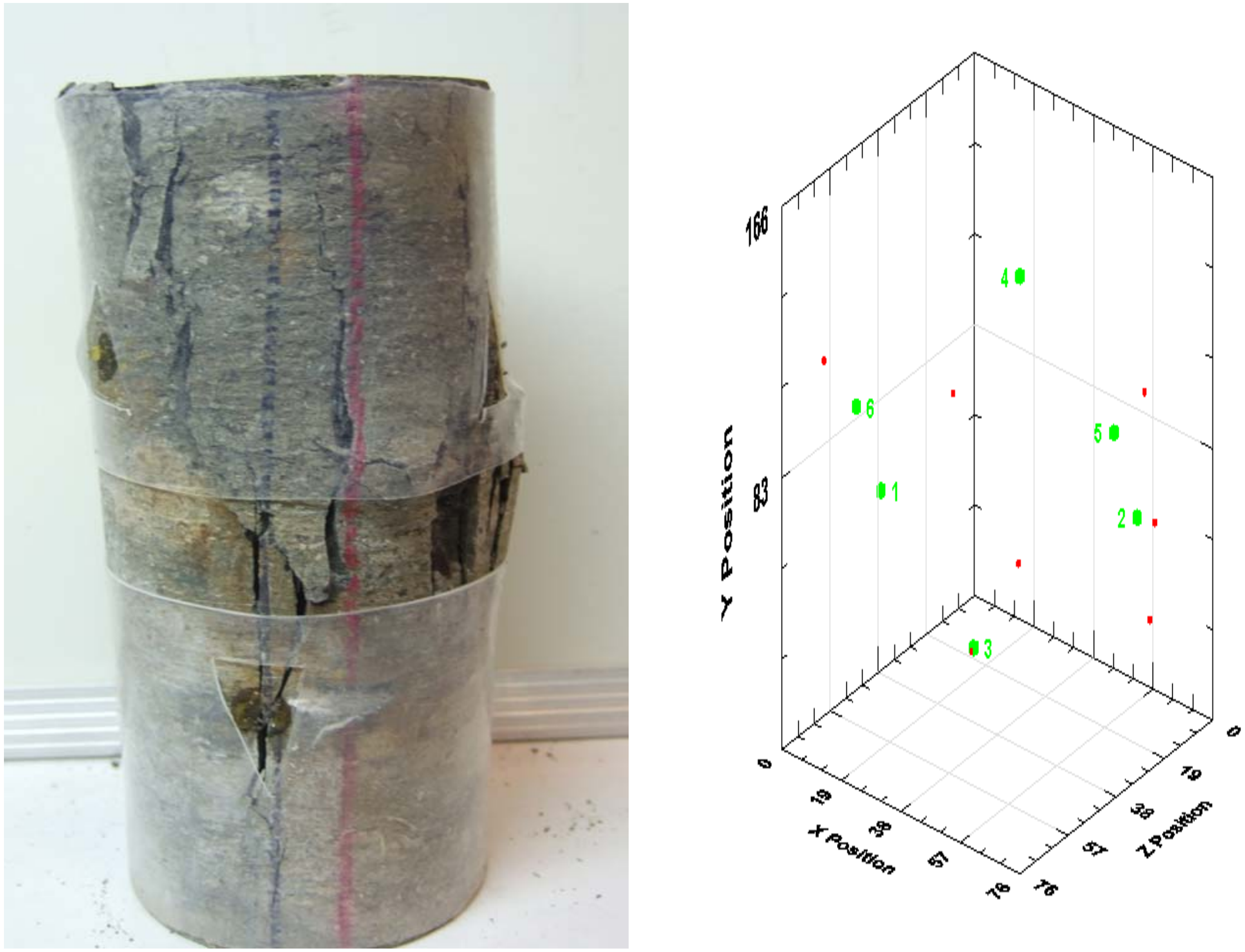

Figure C-3 UCS Specimen DGR4 682.22 m

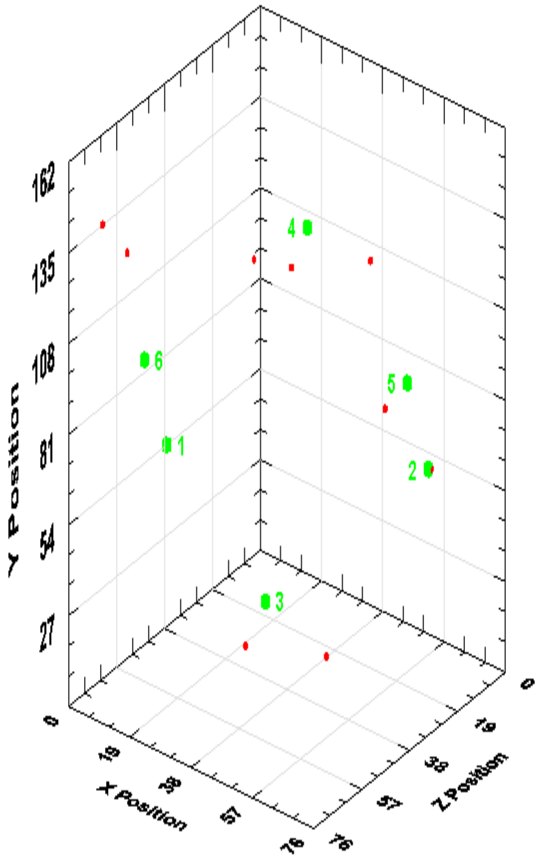

Figure C-4 UCS Specimen DGR5 711.96 m

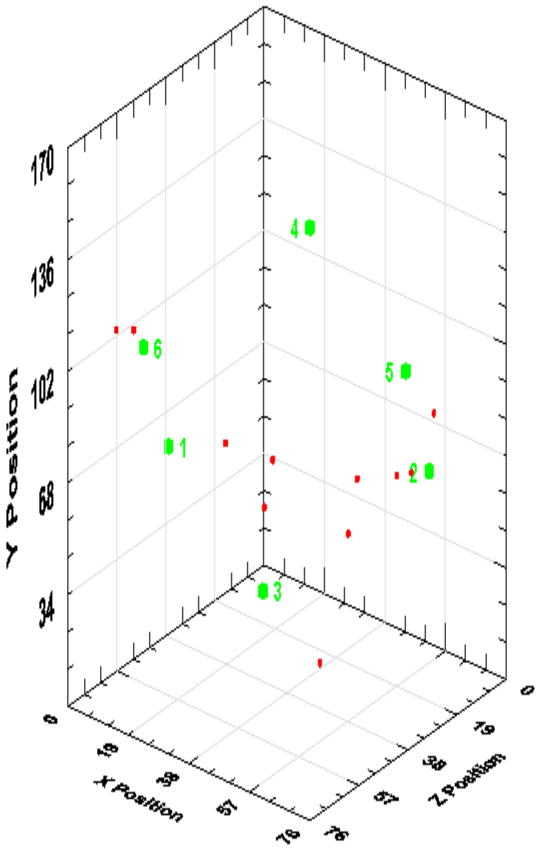

Figure C-5 UCS Specimen DGR5 719.38 m

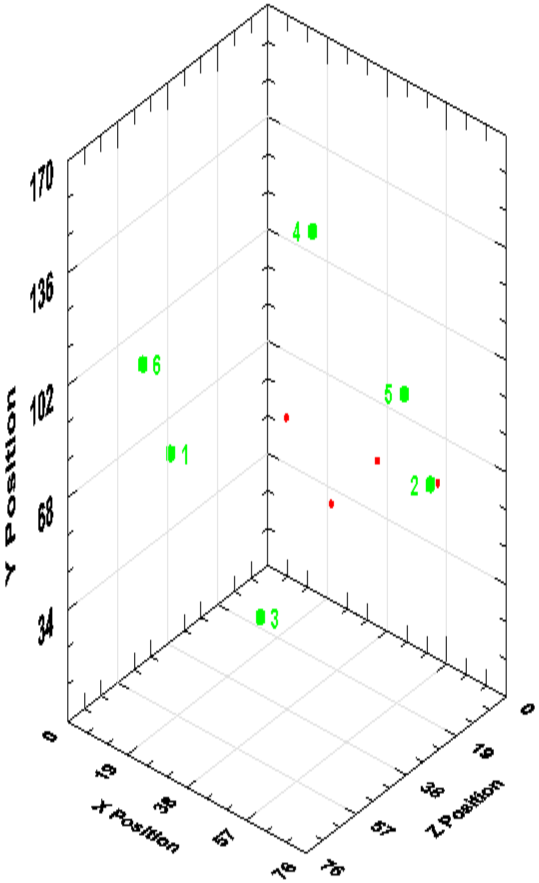

Figure C-6 UCS Specimen DGR5 731.27 m

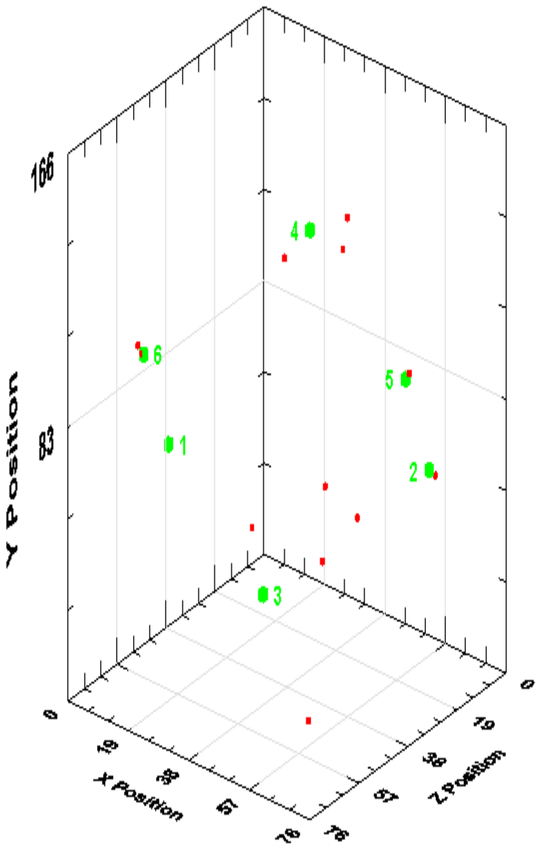

Figure C-7 UCS Specimen DGR5 735.61 m

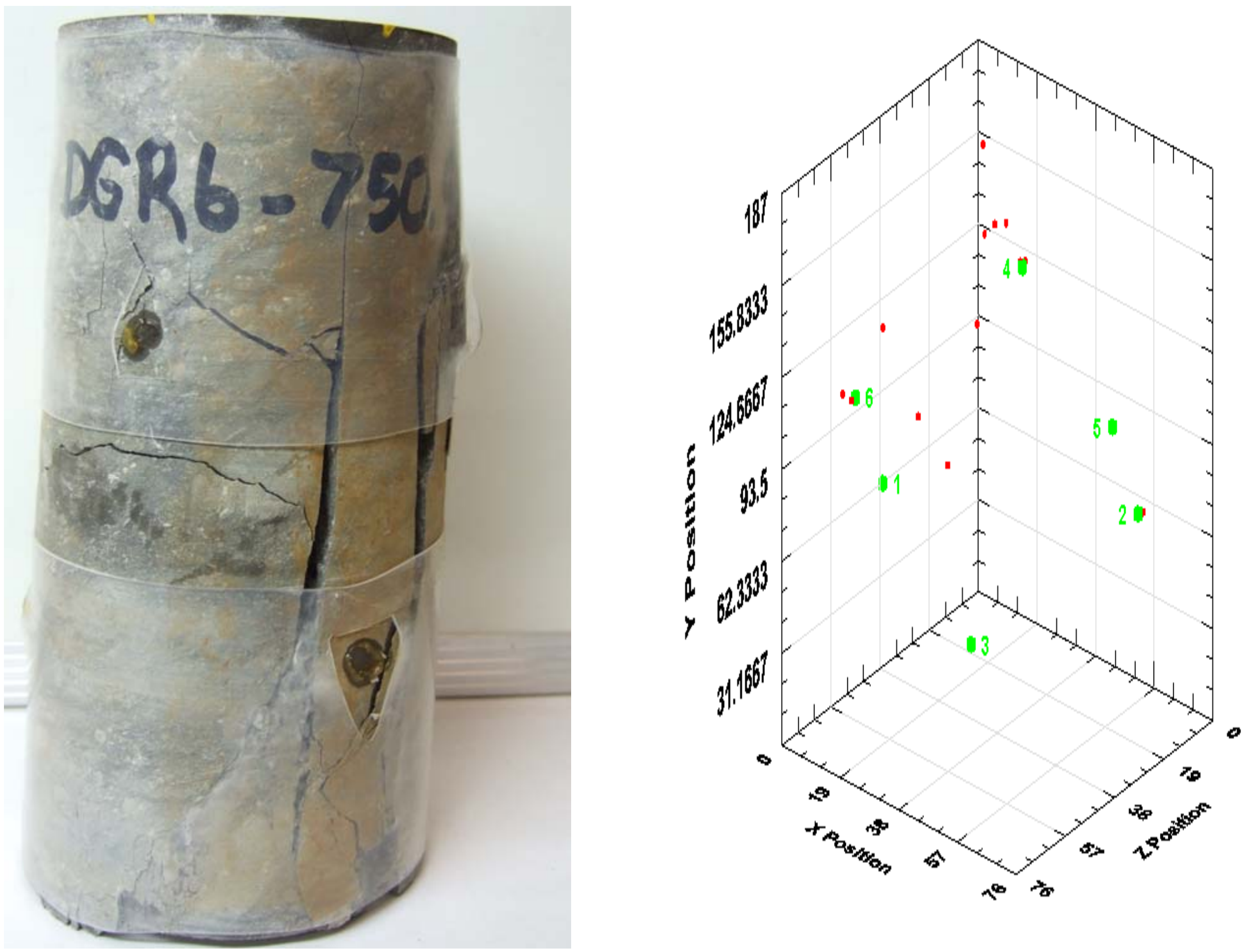

Figure C-8 UCS Specimen DGR6 747.99 m

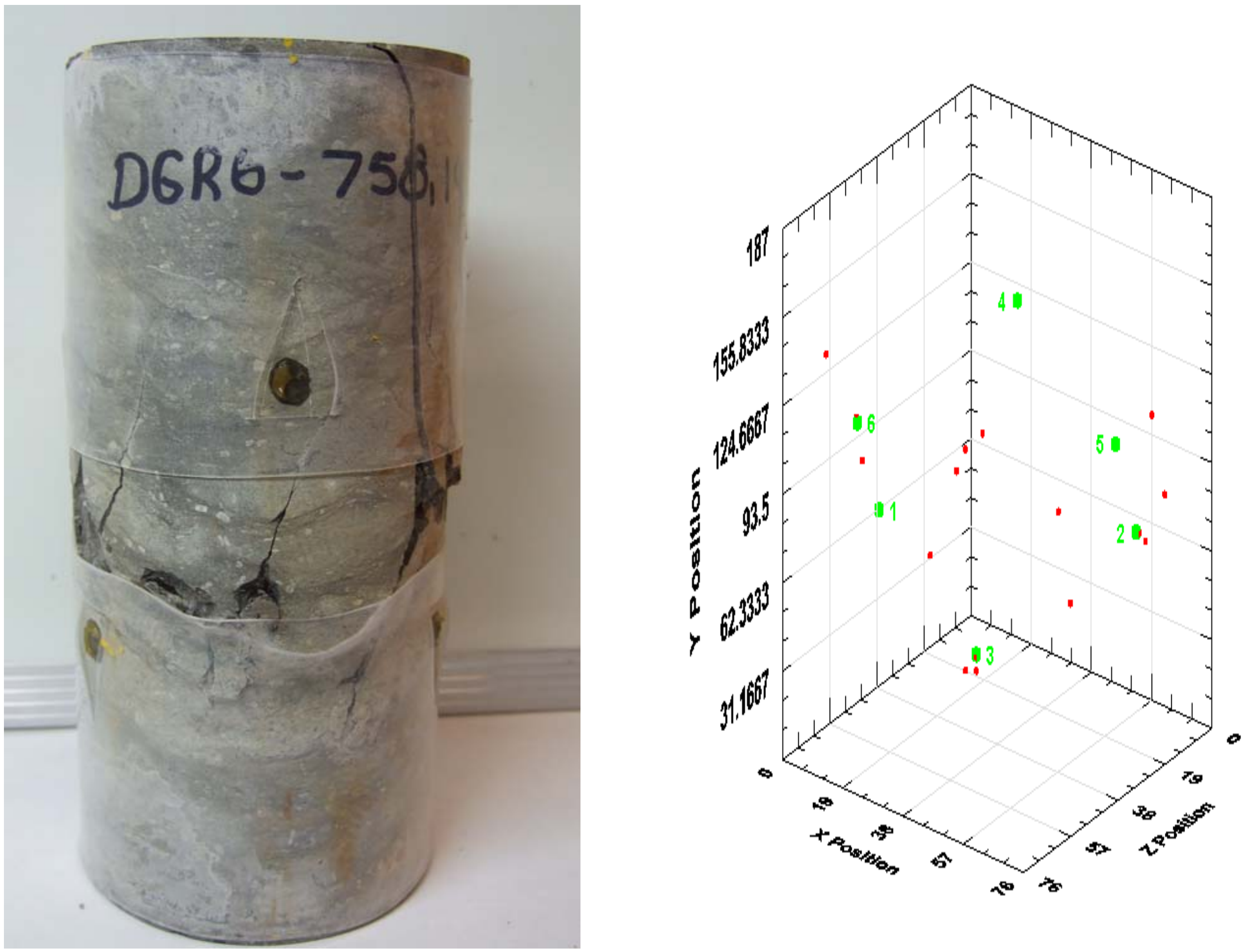

Figure C-9 UCS Specimen DGR6 755.19 m

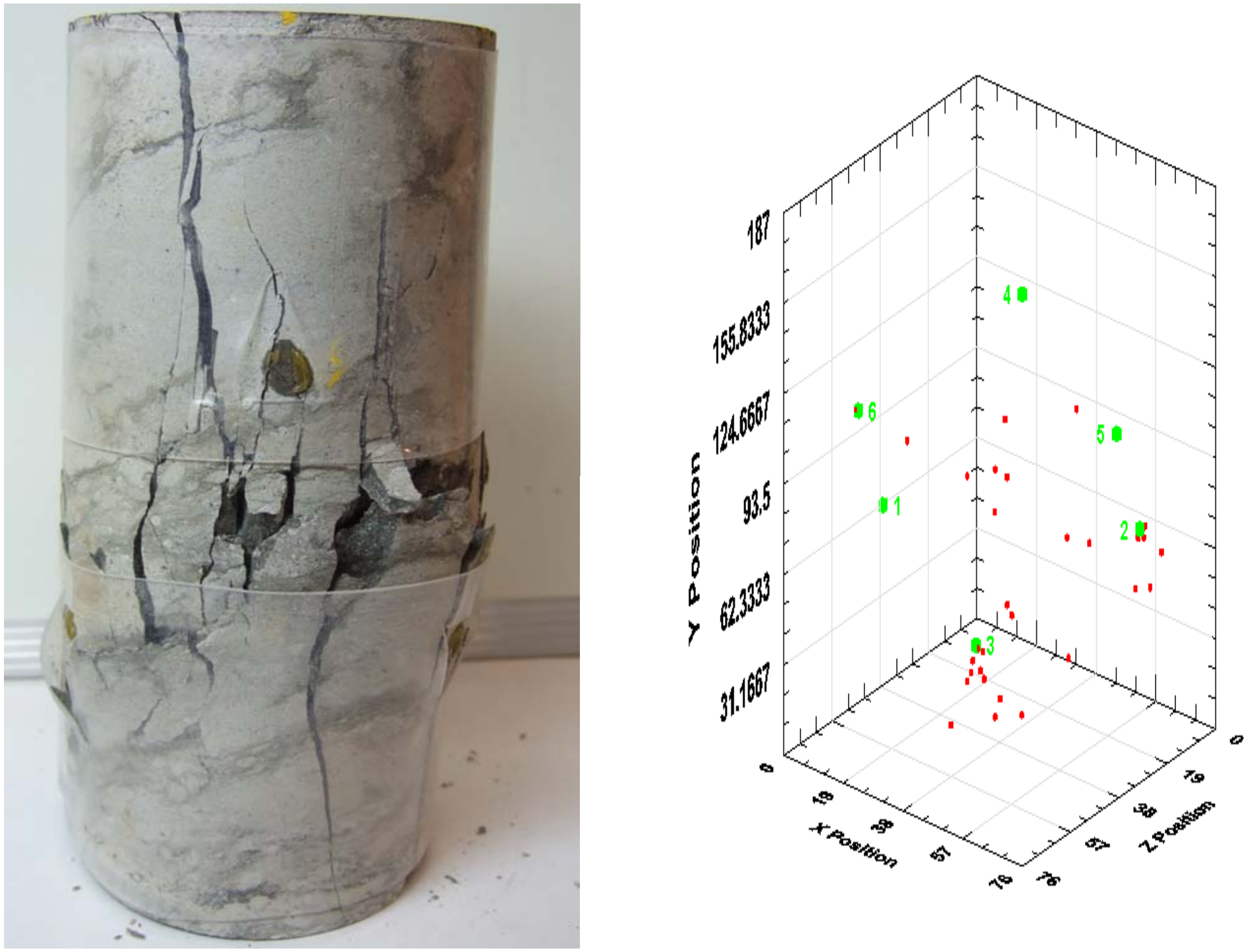

Figure C-10 UCS Specimen DGR6 770.07 m

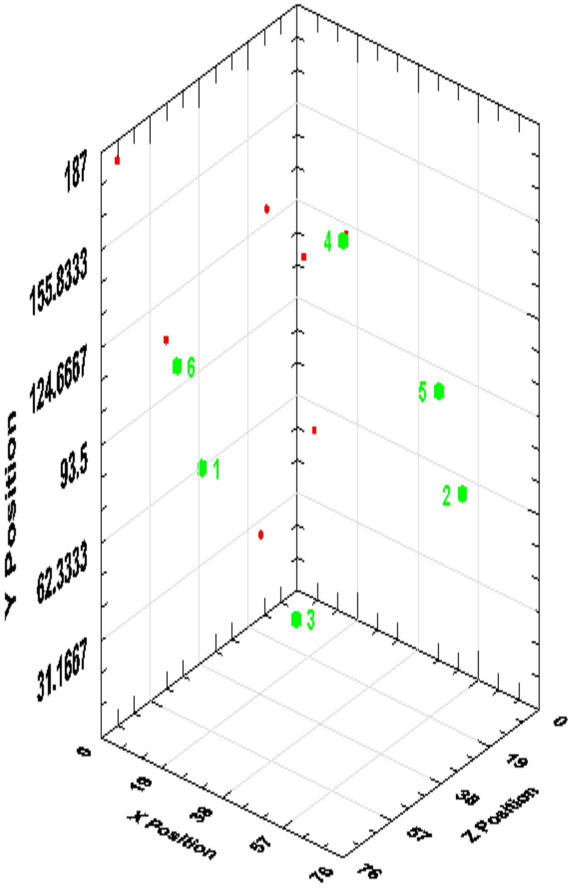

Figure C-11 UCS Specimen DGR6 773.82 m

Figure C-12 UCS Specimen DGR4 727.95 m

Figure C-13 UCS Specimen DGR4 730.55 m

Figure C-14 UCS Specimen DGR4 771.71 m

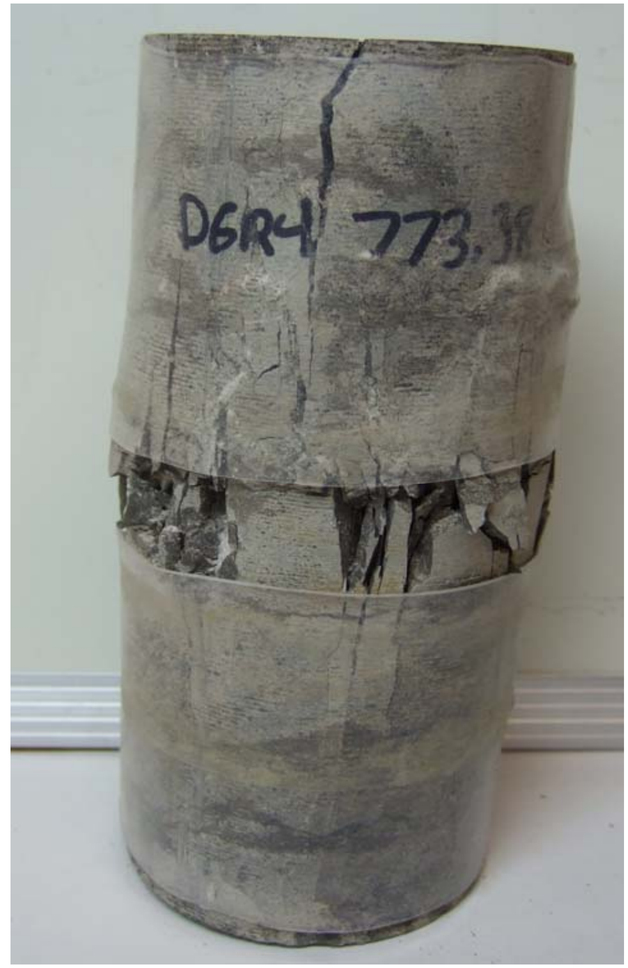

Figure C-15 UCS Specimen DGR4 773.38 m

Figure C-16 UCS Specimen DGR4 808.56 m

Figure C-17 UCS Specimen DGR4 809.88 m

Figure C-18 UCS Specimen DGR4 856.29 m

Figure C-19 UCS Specimen DGR4 856.80 m

APPENDIX D

Stress-Strain Curves of Triaxial Tests

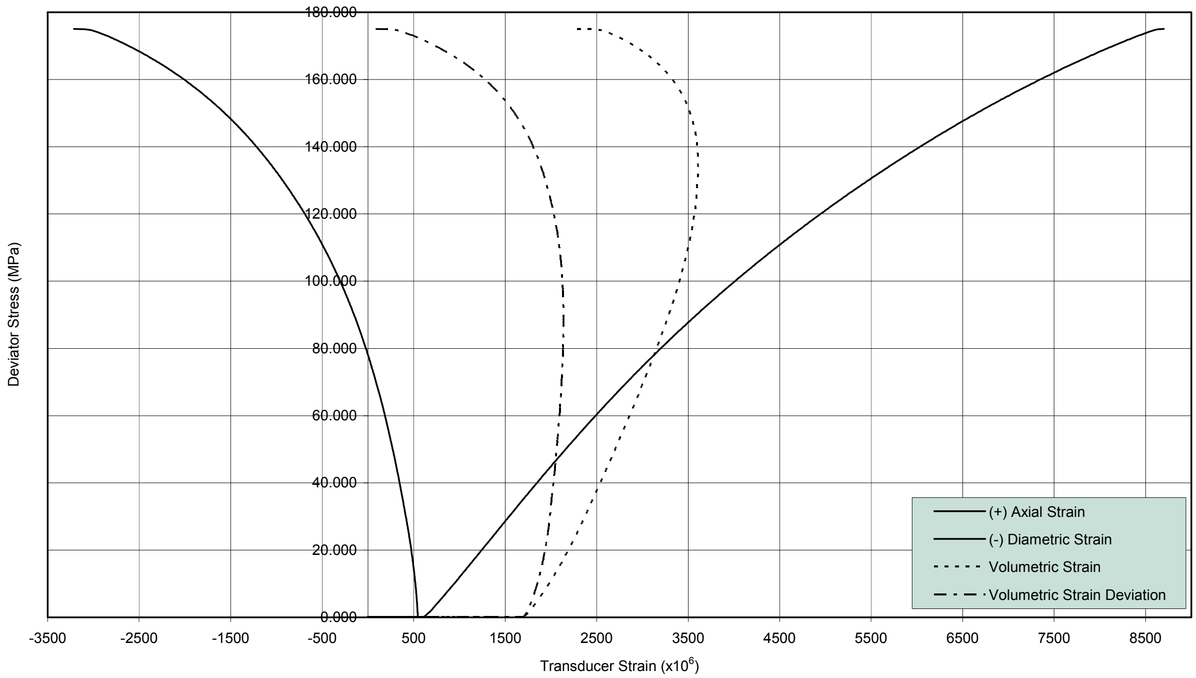

Figure D-1 TCS Specimen DGR-5, 700.65 m

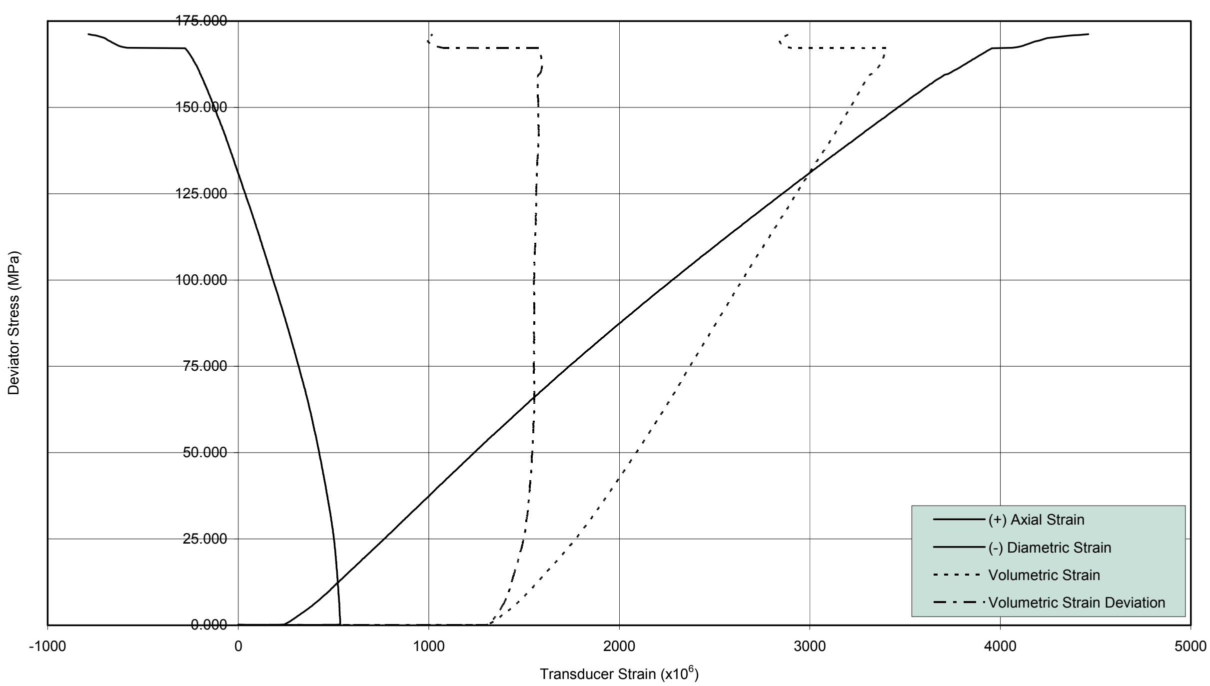

Figure D-2 TCS Specimen DGR-5, 702.81 m

APPENDIX E

Failed Triaxial Specimens

Figure E-1 DGR-5 700.65 m

Figure E-2 DGR-5 702.81 m

APPENDIX F

Shear Stress vs Displacement
Shear Stress vs Normal Stress
Normal Stress vs Displacement

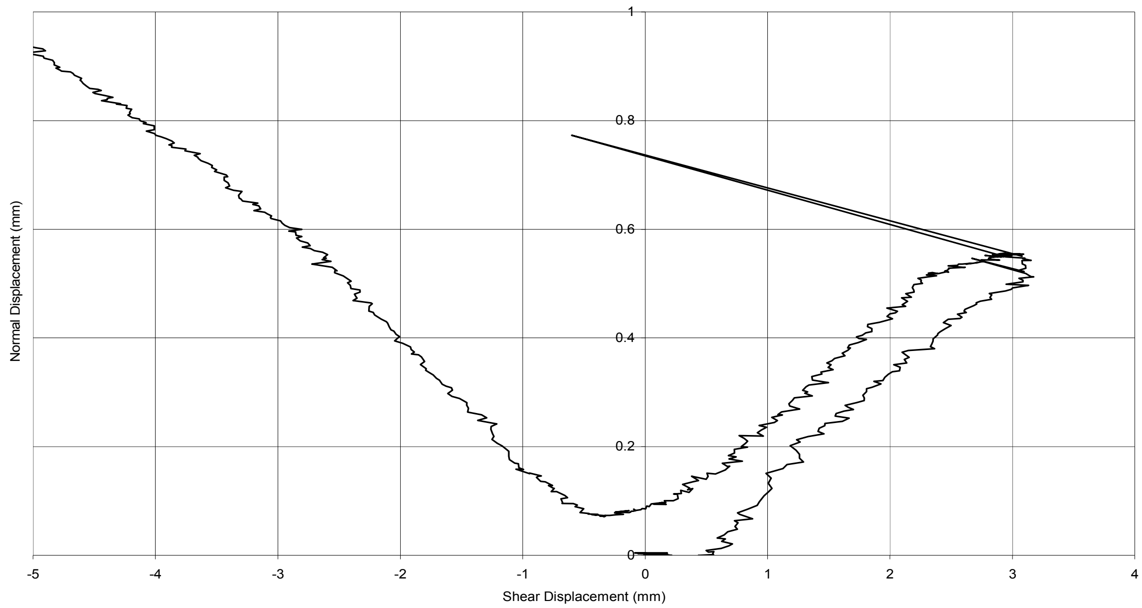

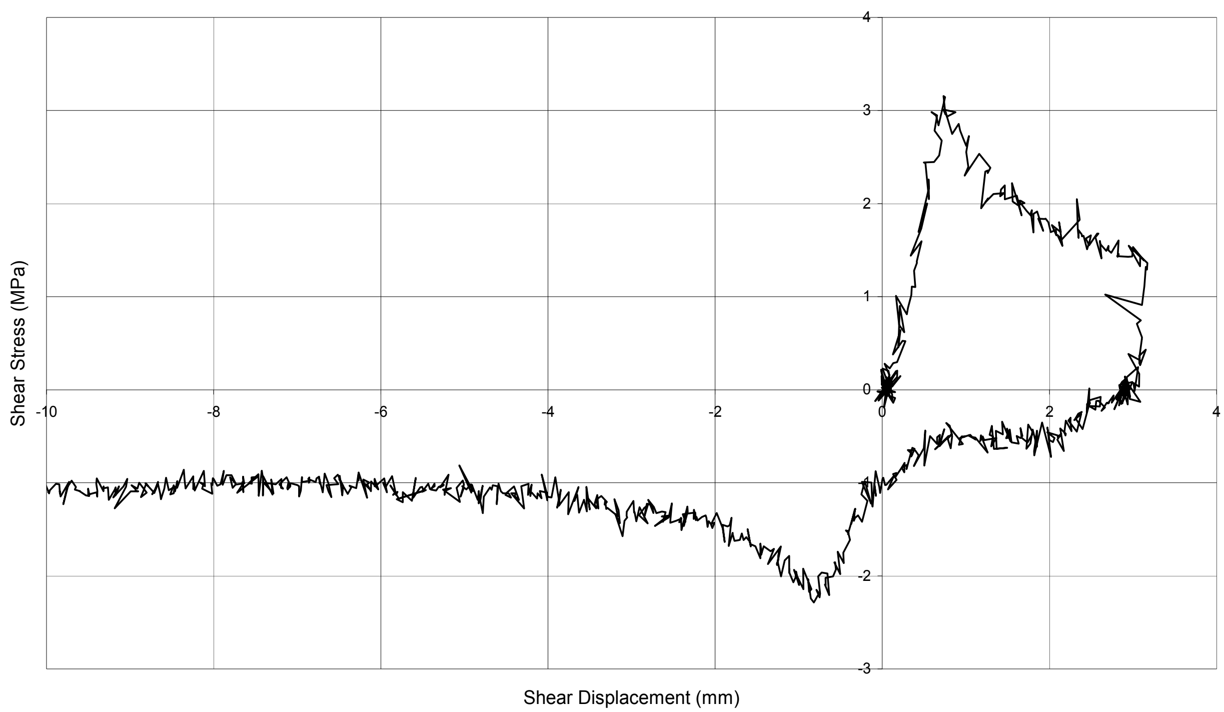

Figure F-1 DGR-2, 654.00 m

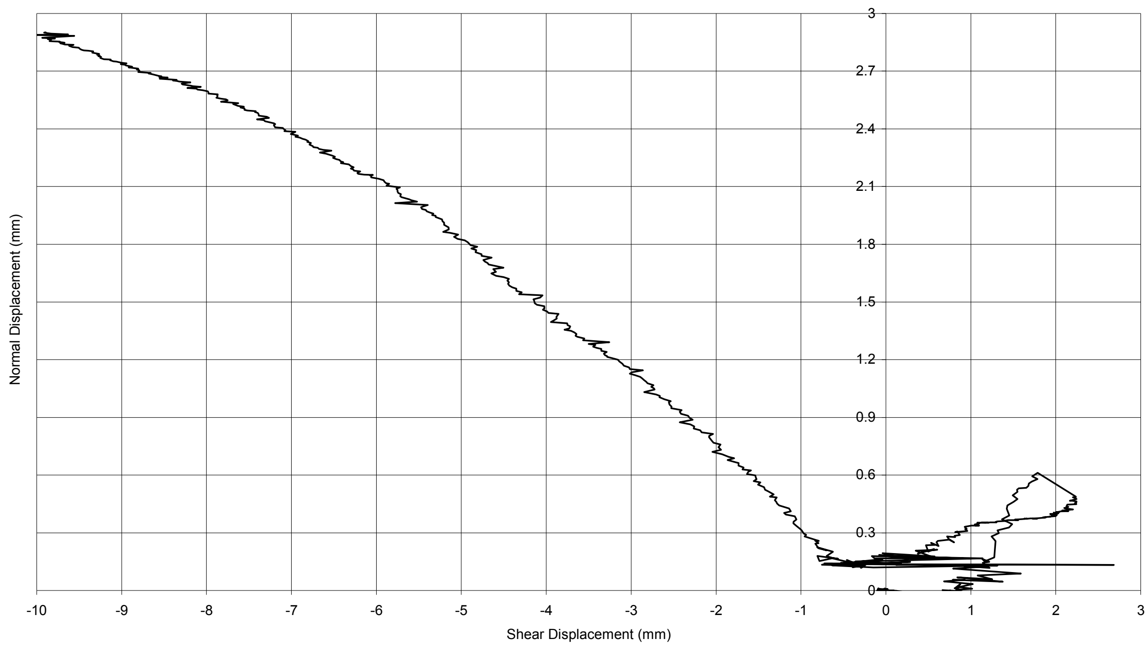

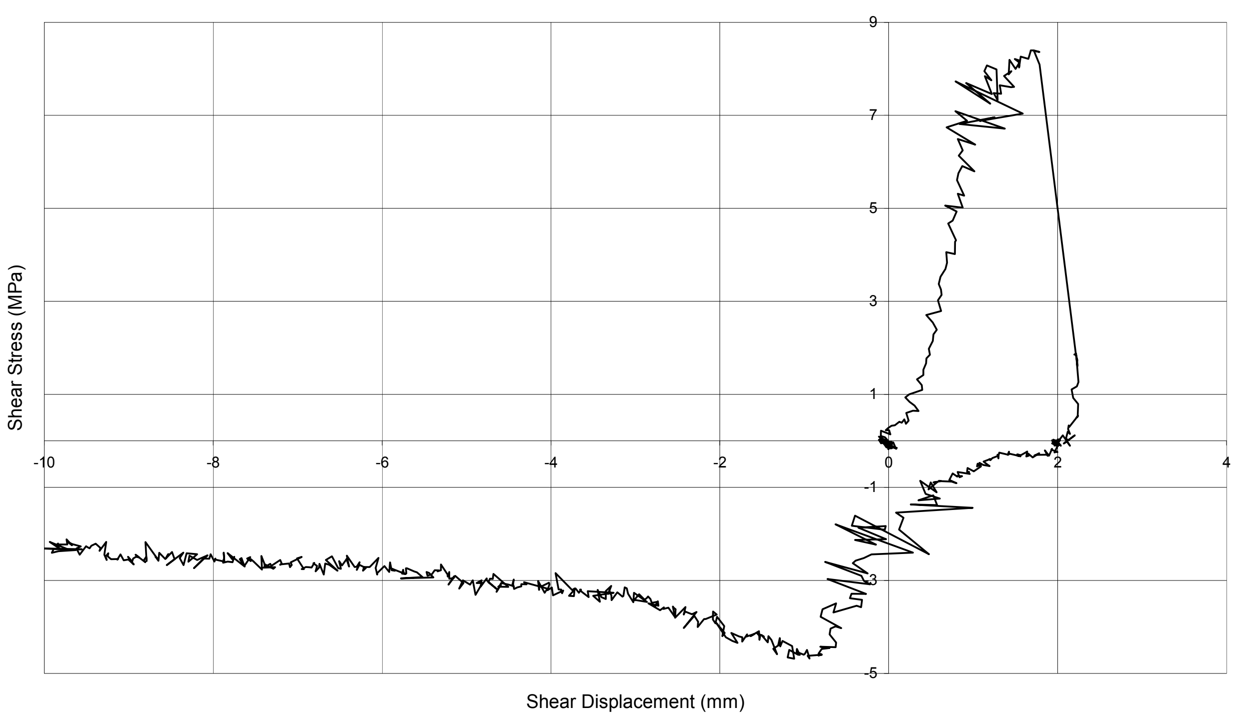

Figure F-2 DGR-2, 661.36 m

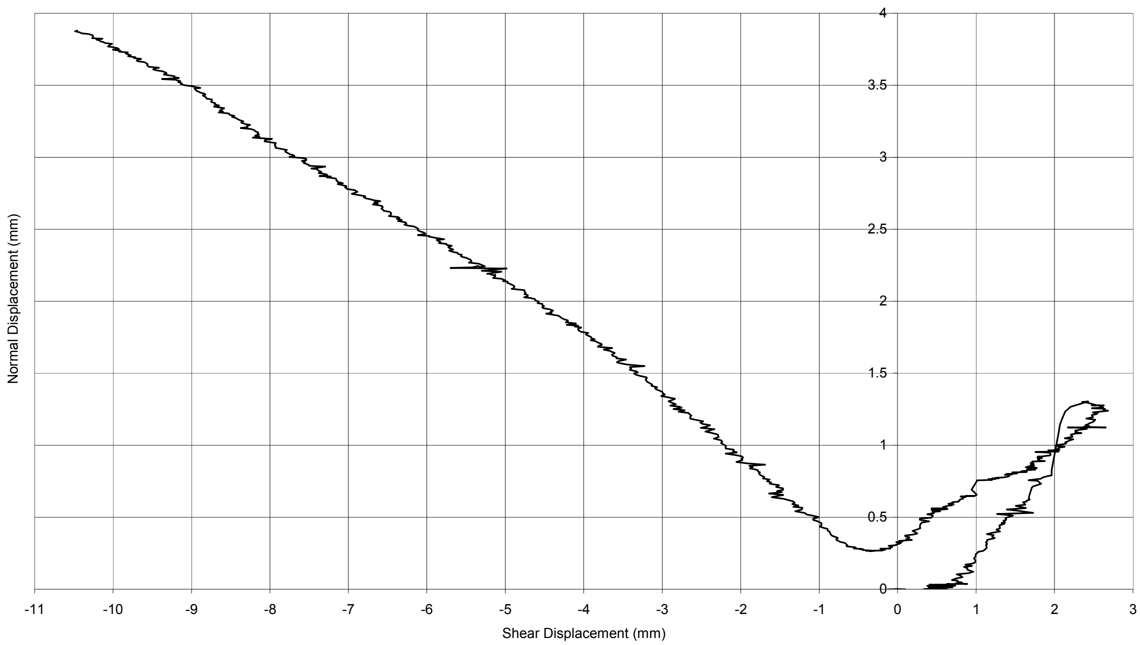

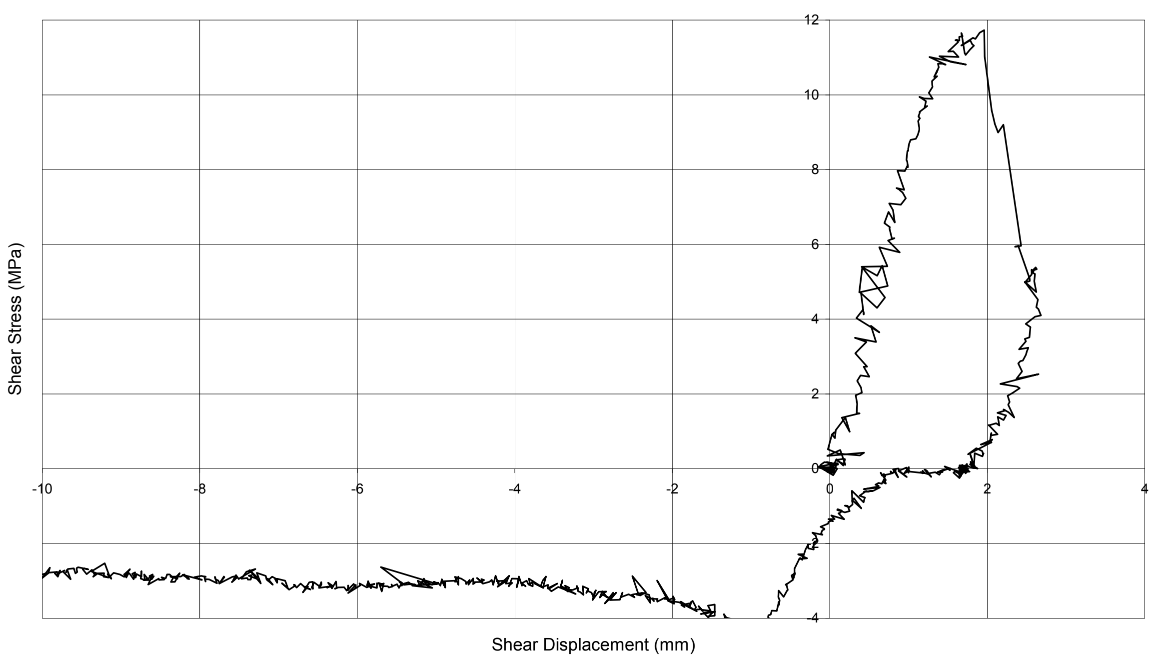

Figure F-3 DGR-2, 665.29 m

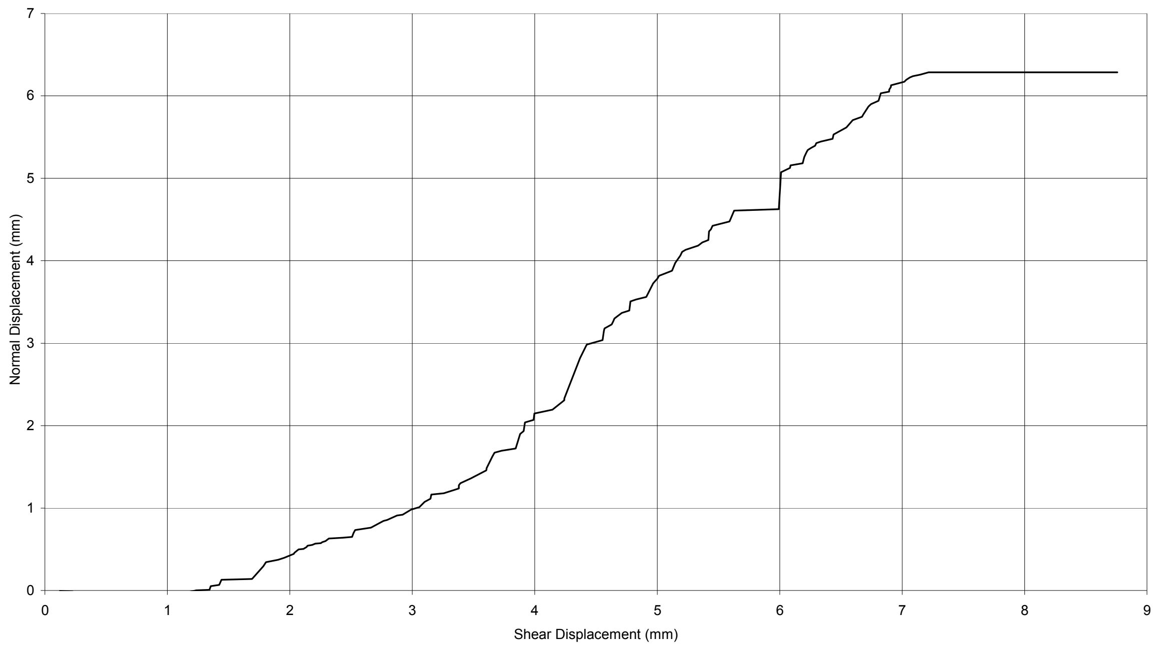

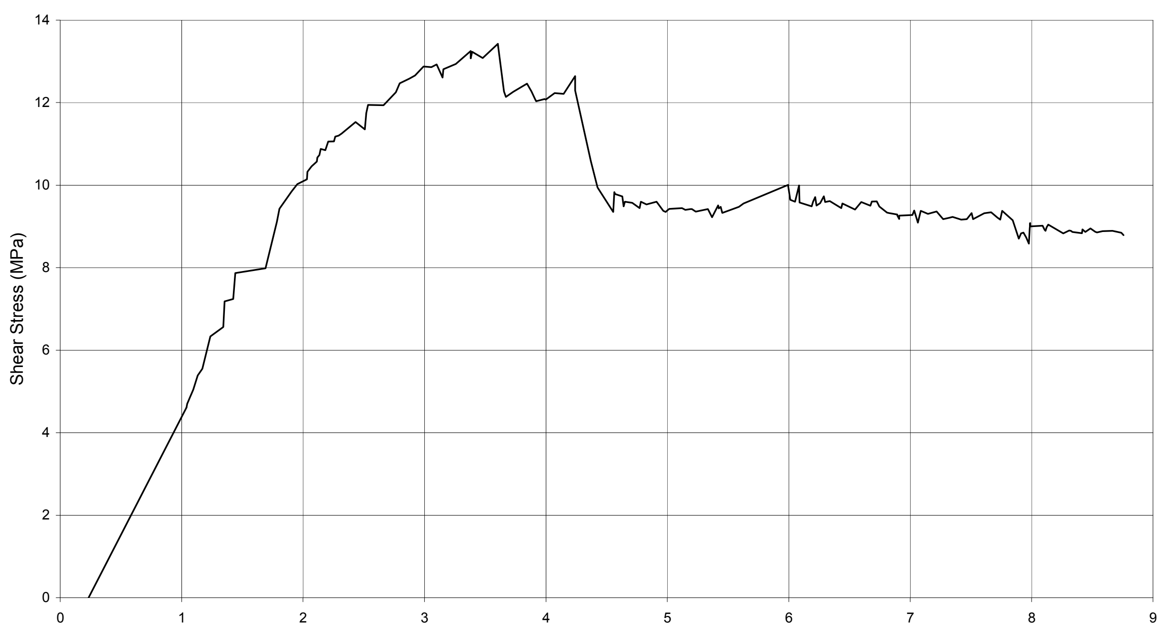

Figure F-4 DGR-3, 666.10 m

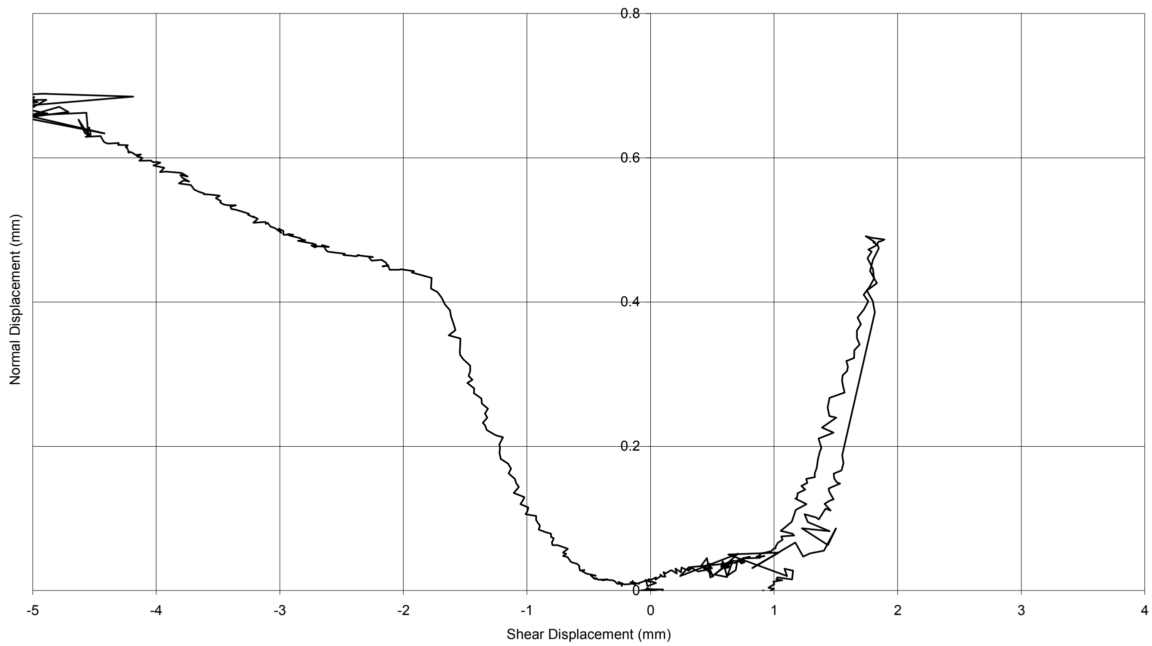

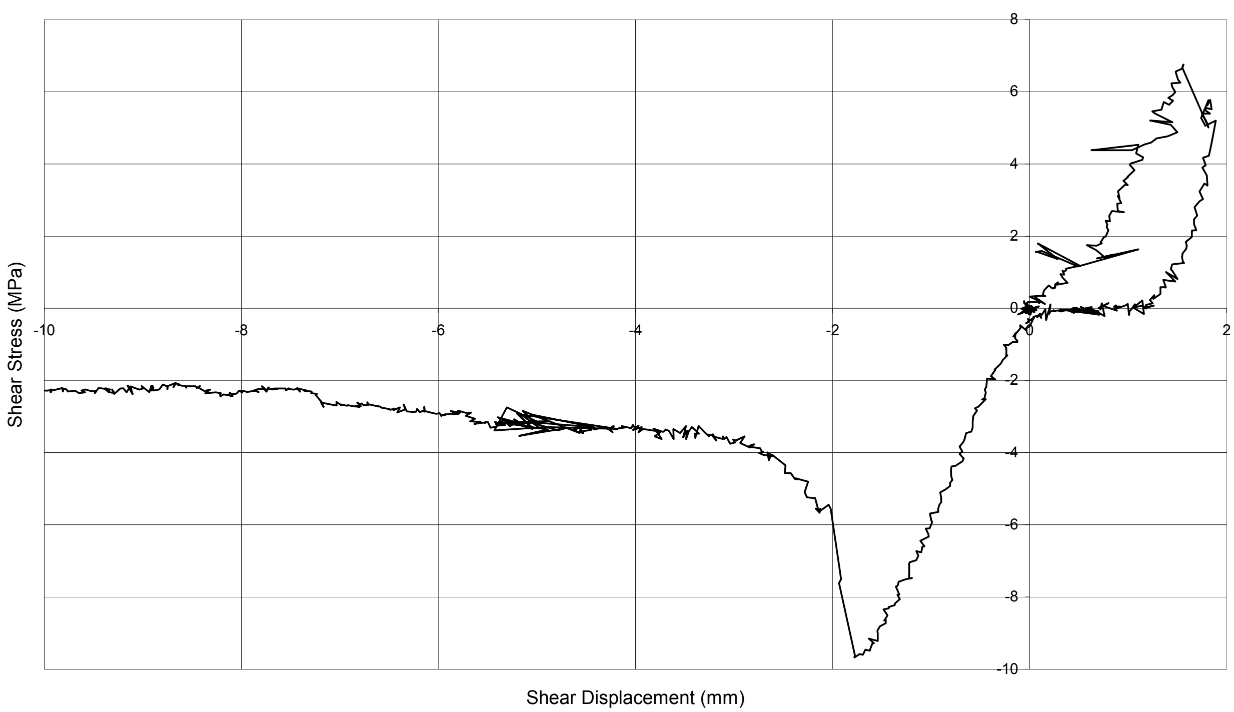

Figure F-5 DGR-4, 652.93 m

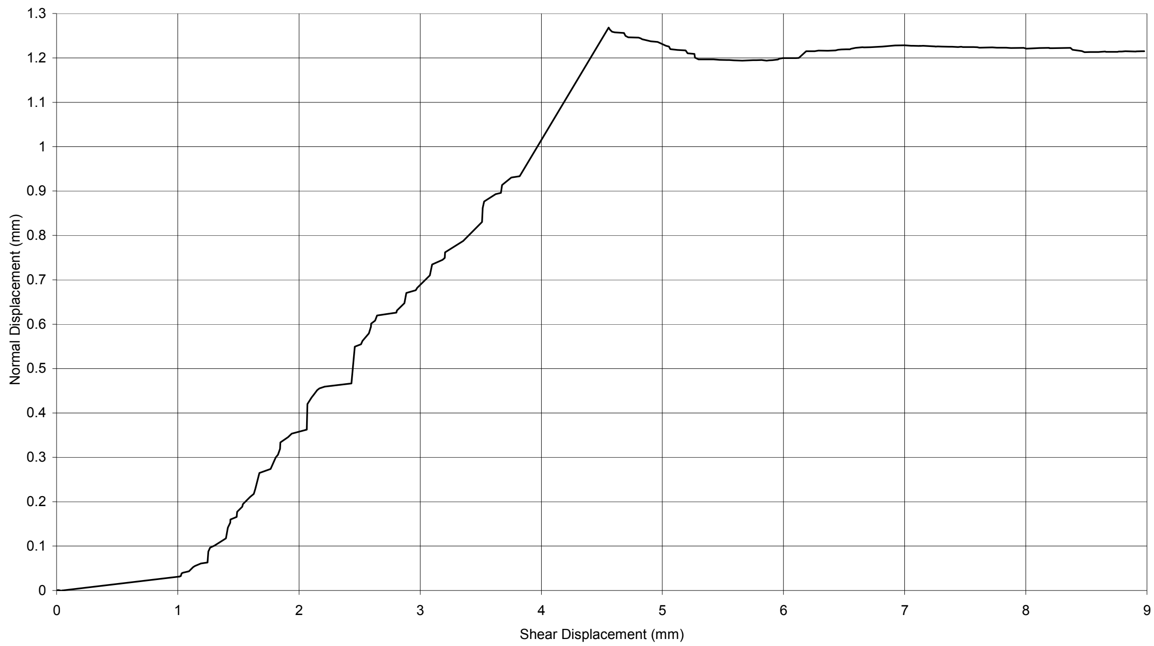

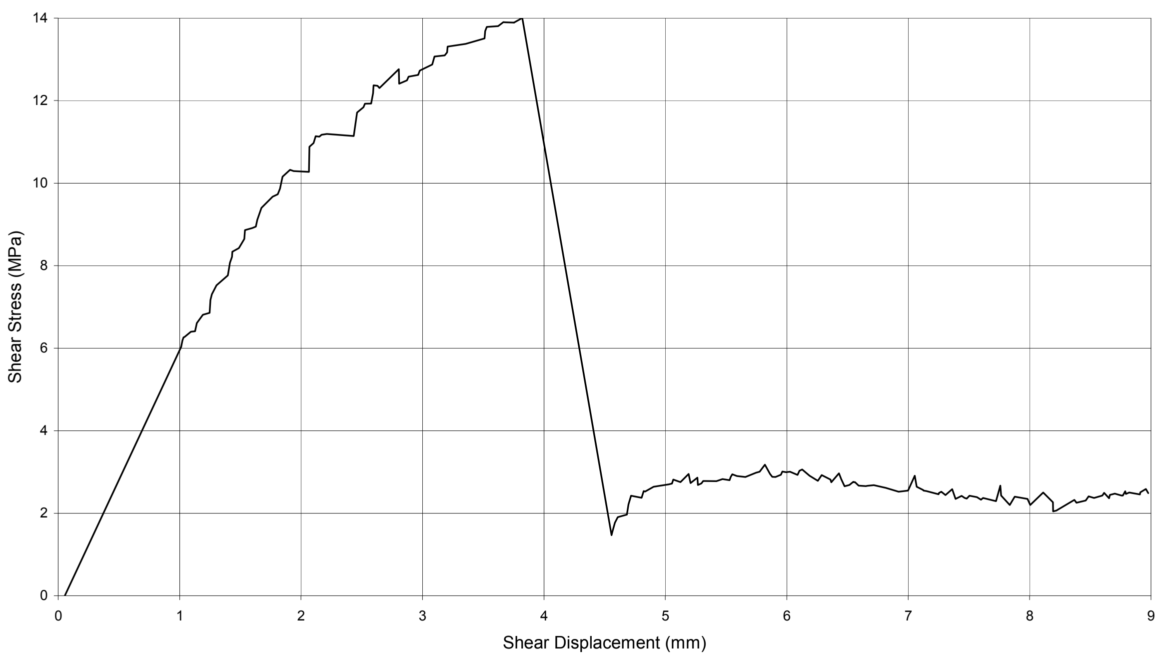

Figure F-6 DGR-4, 661.90 m

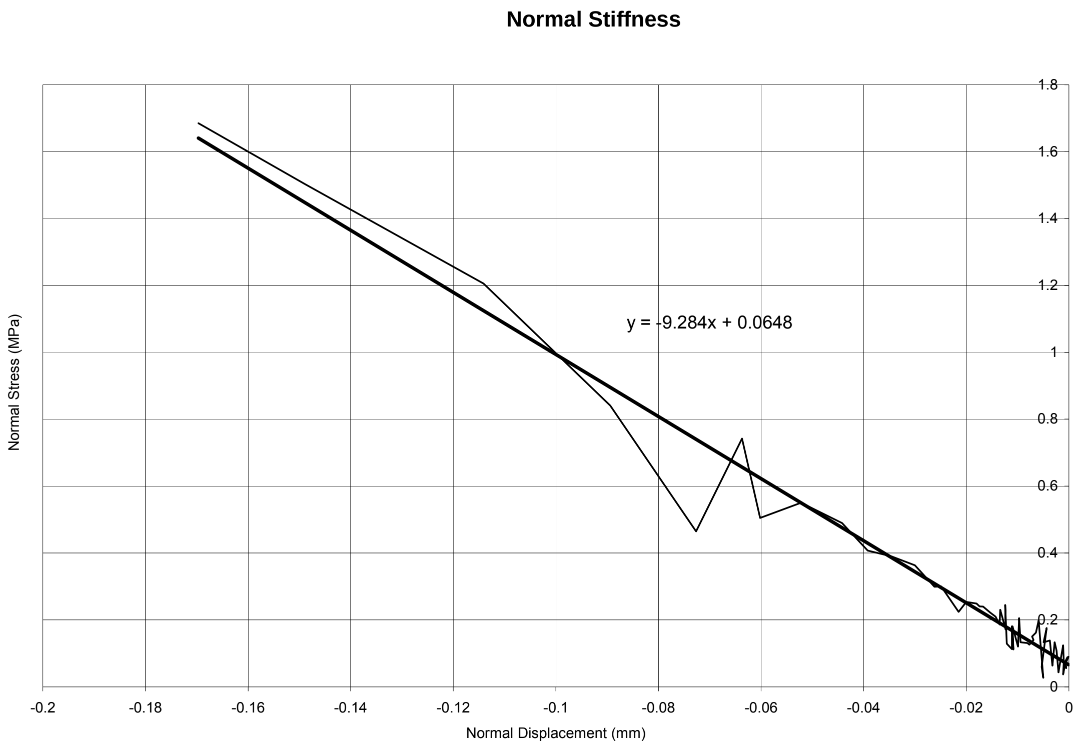

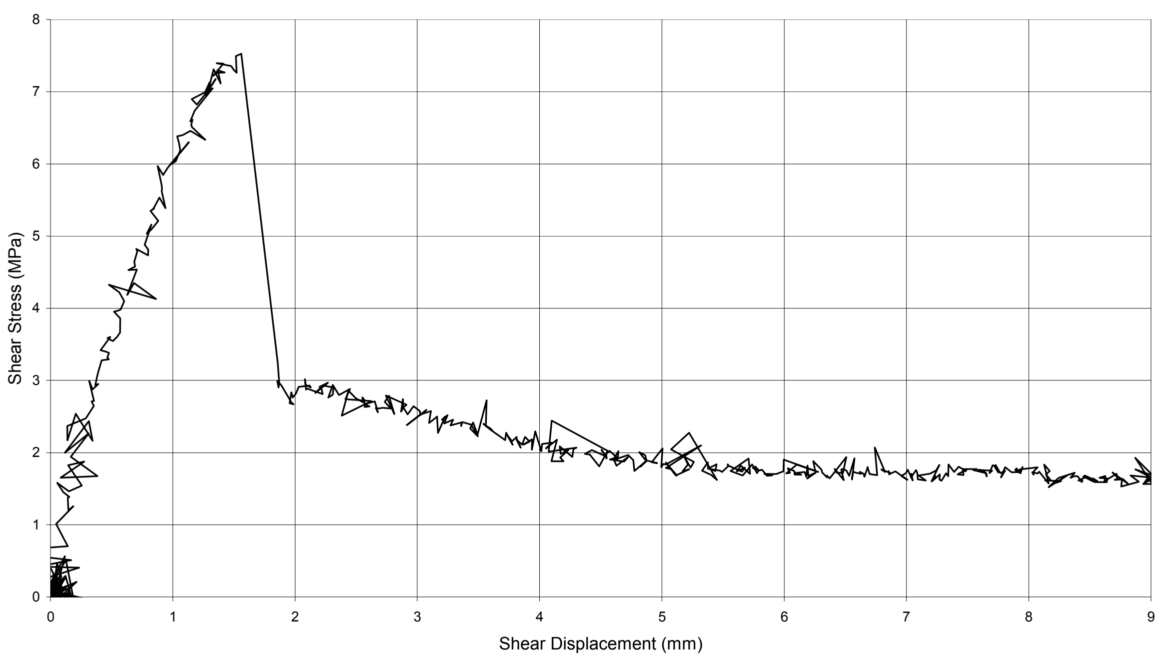

Figure F-7 DGR-5, 700.70 m

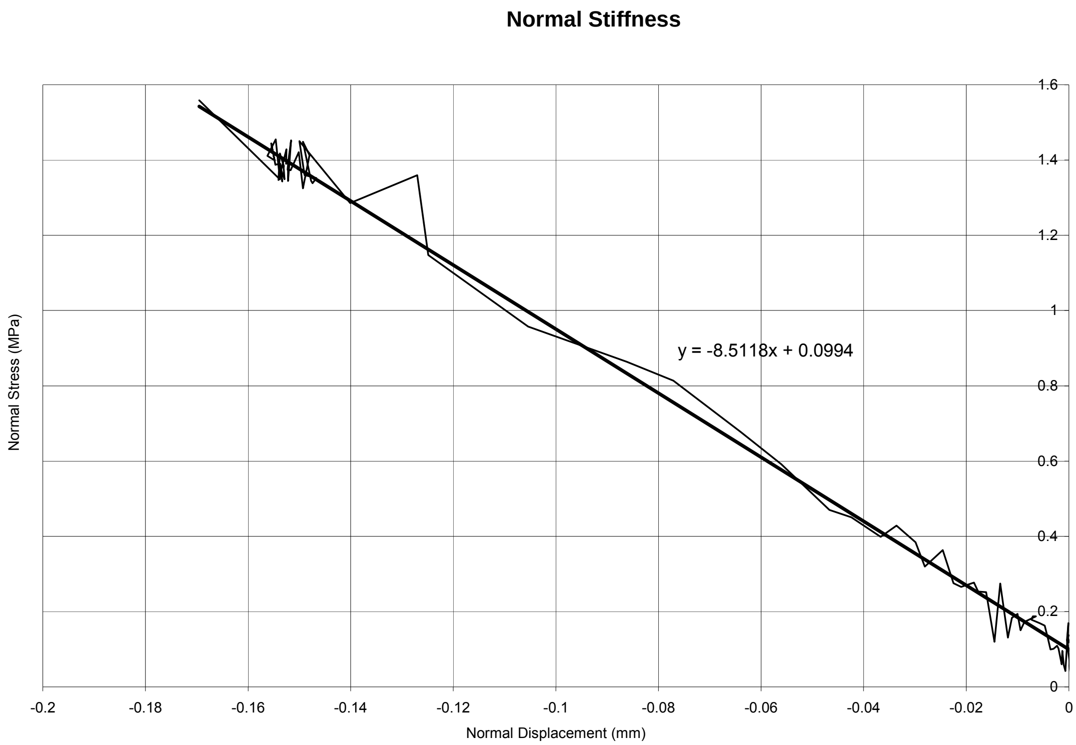

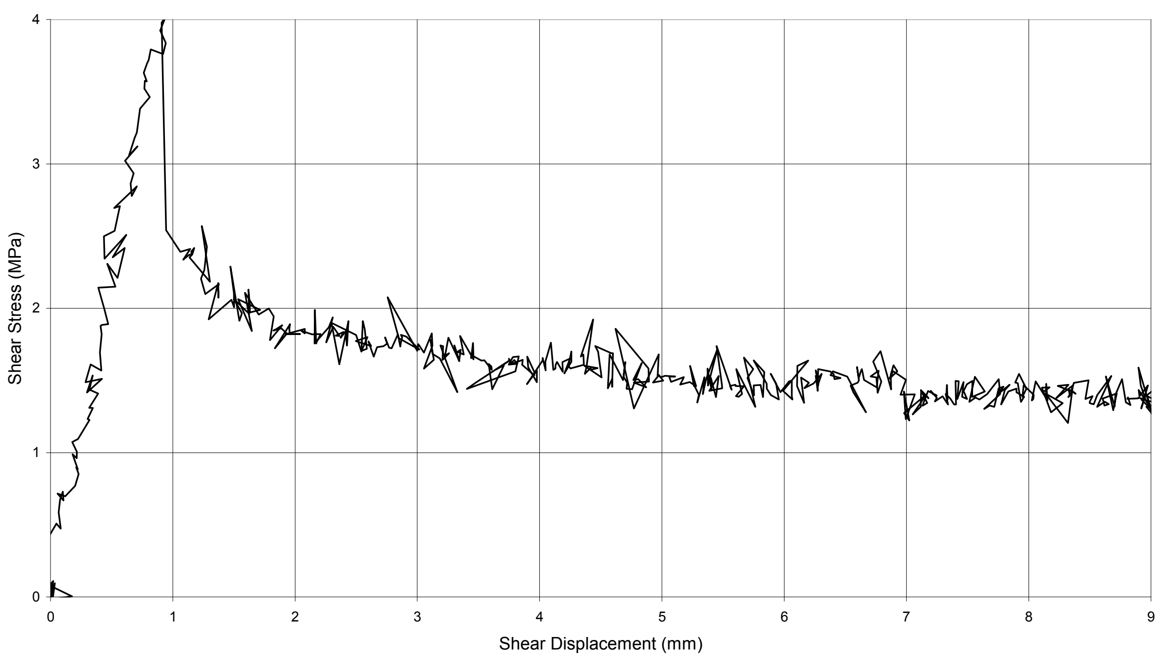

Figure F-8 DGR-5, 705.90 m

Normal Stiffness

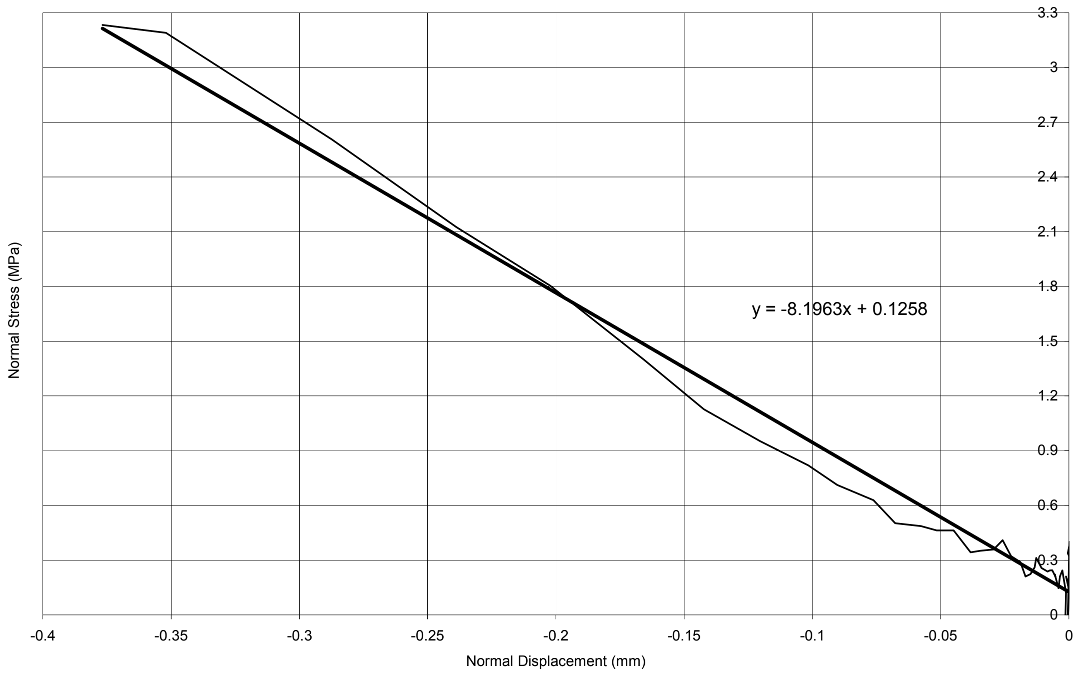

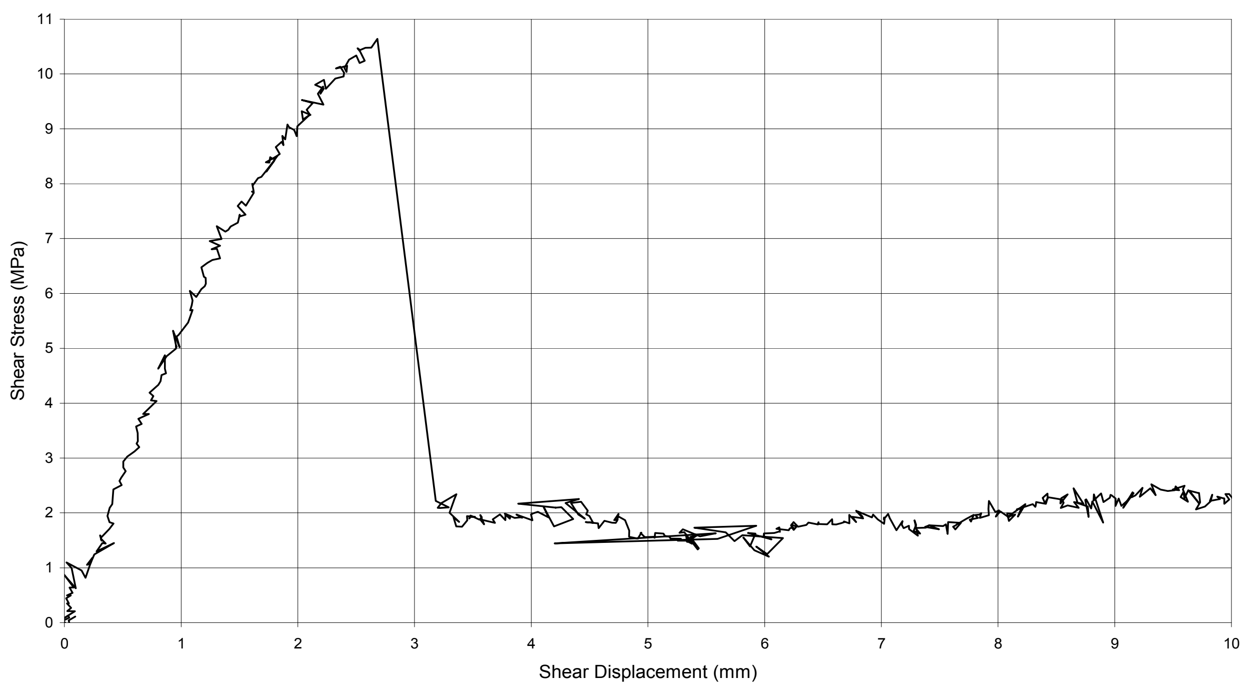

Figure F-9 DGR-5, 719.65 m

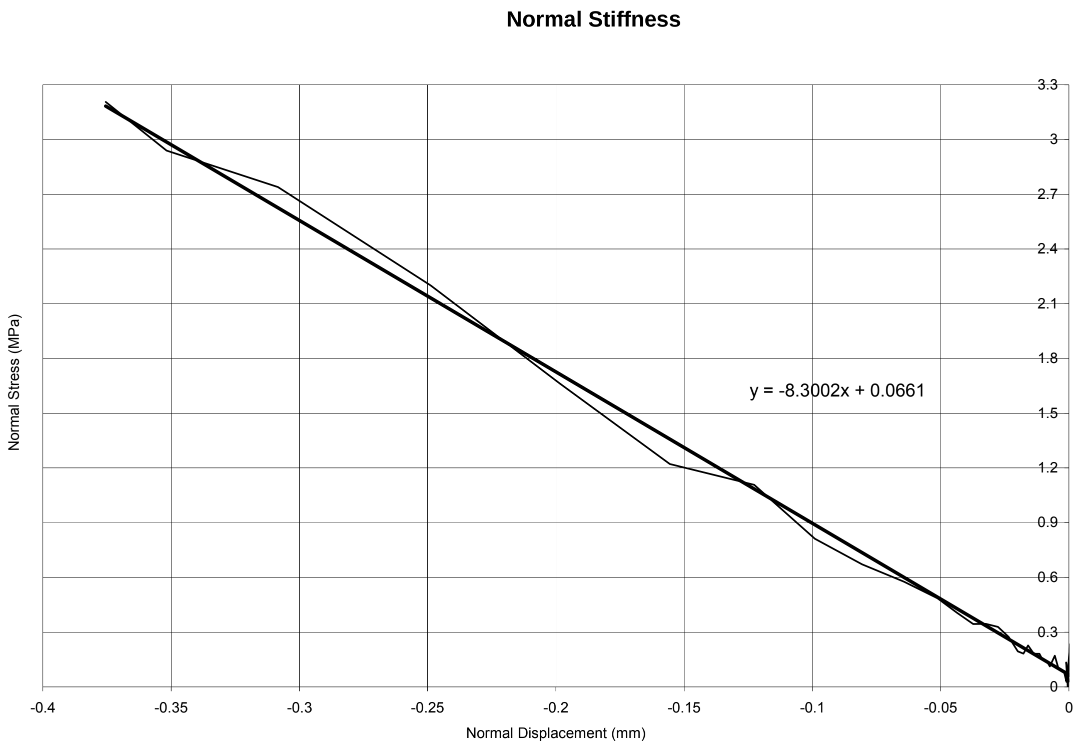

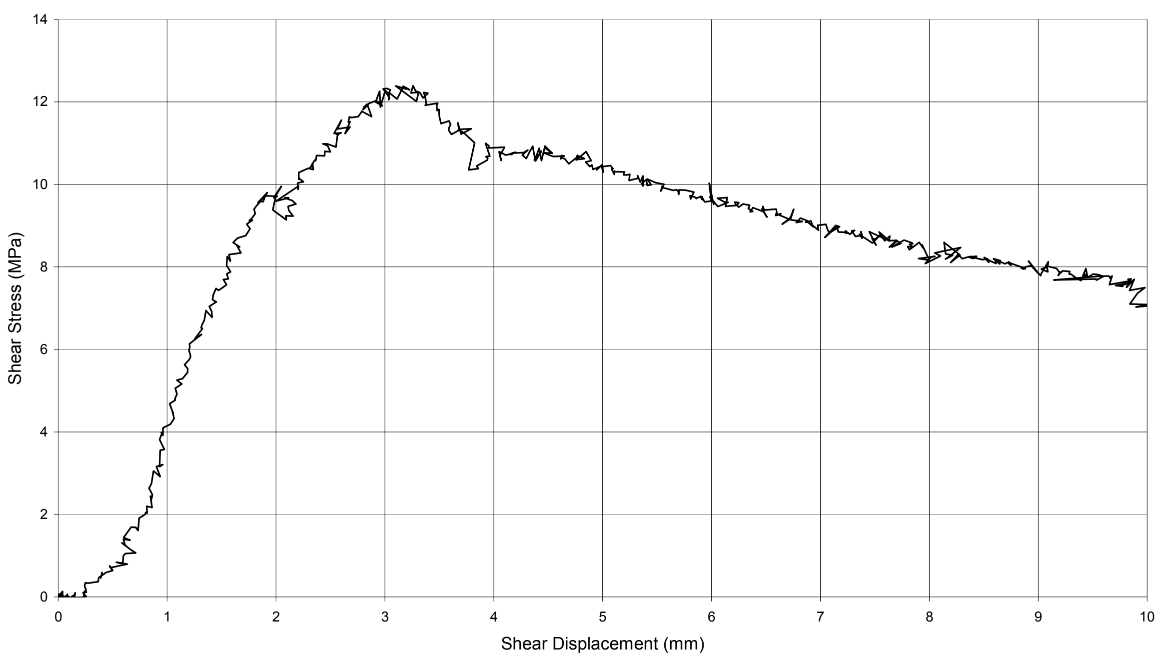

Figure F-10 DGR-5, 725.50 m

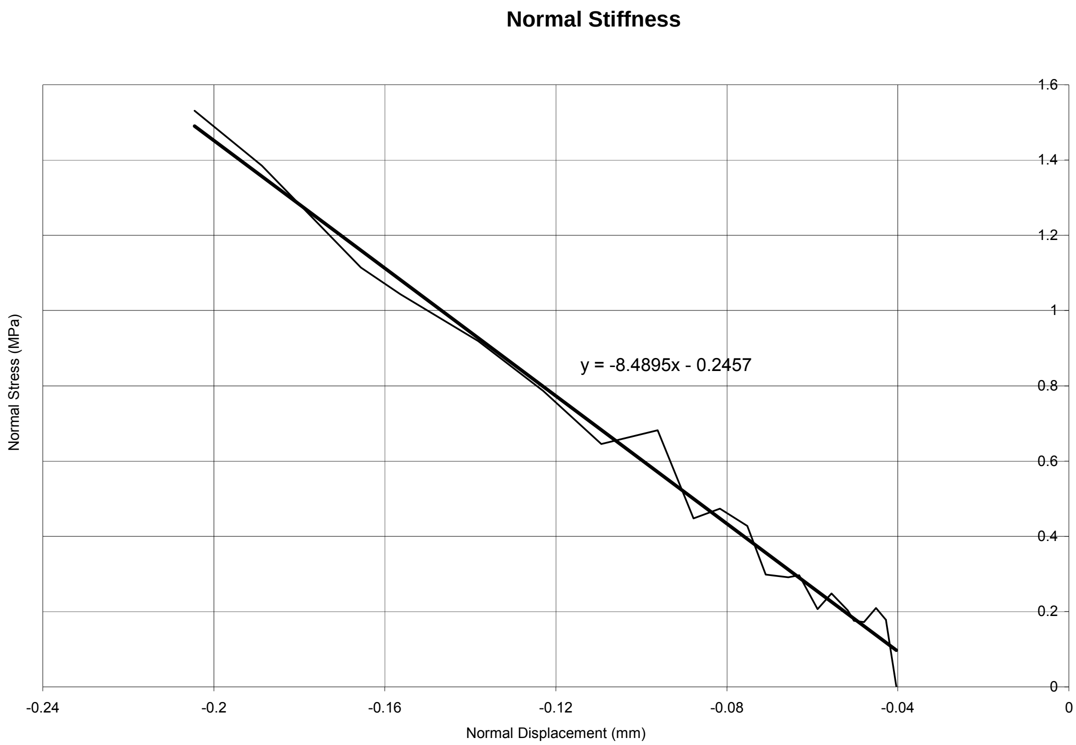

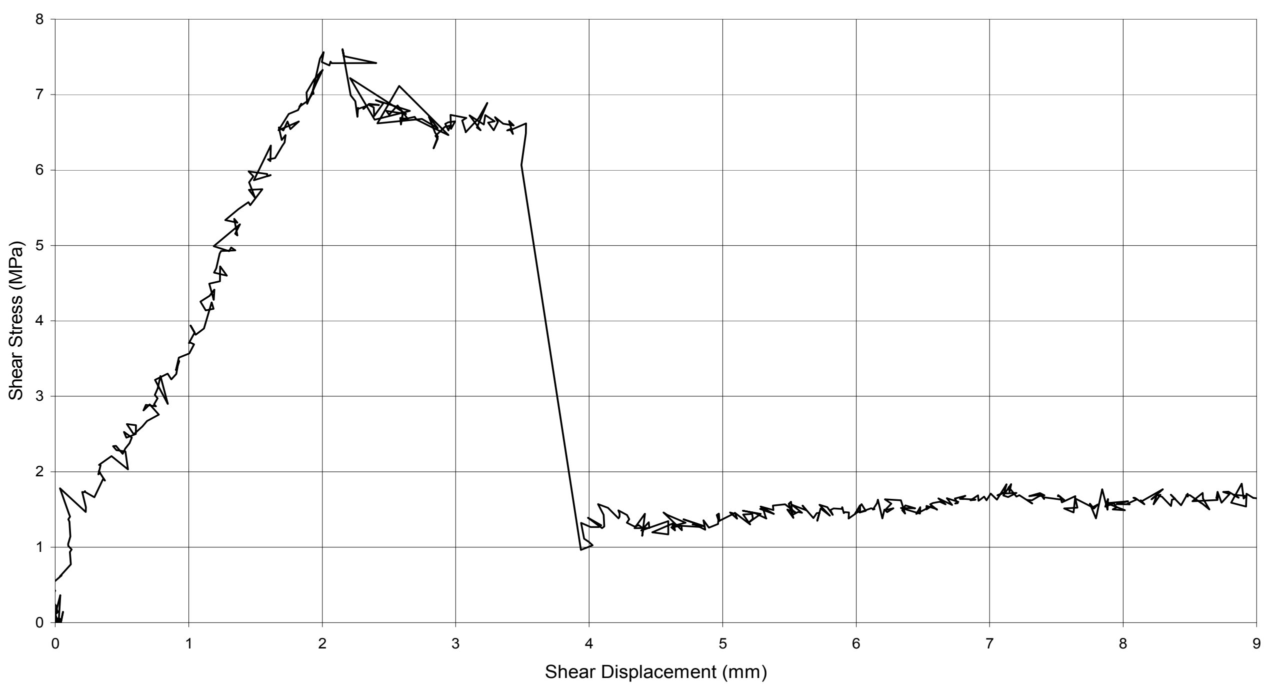

Figure F-11 DGR-5, 729.70 m

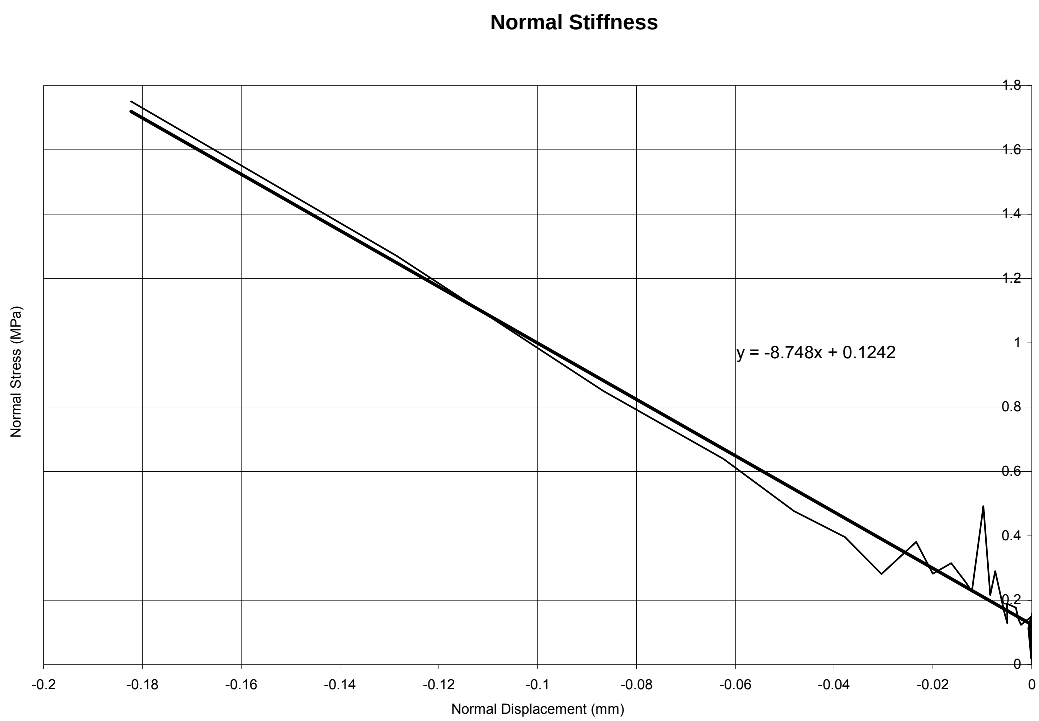

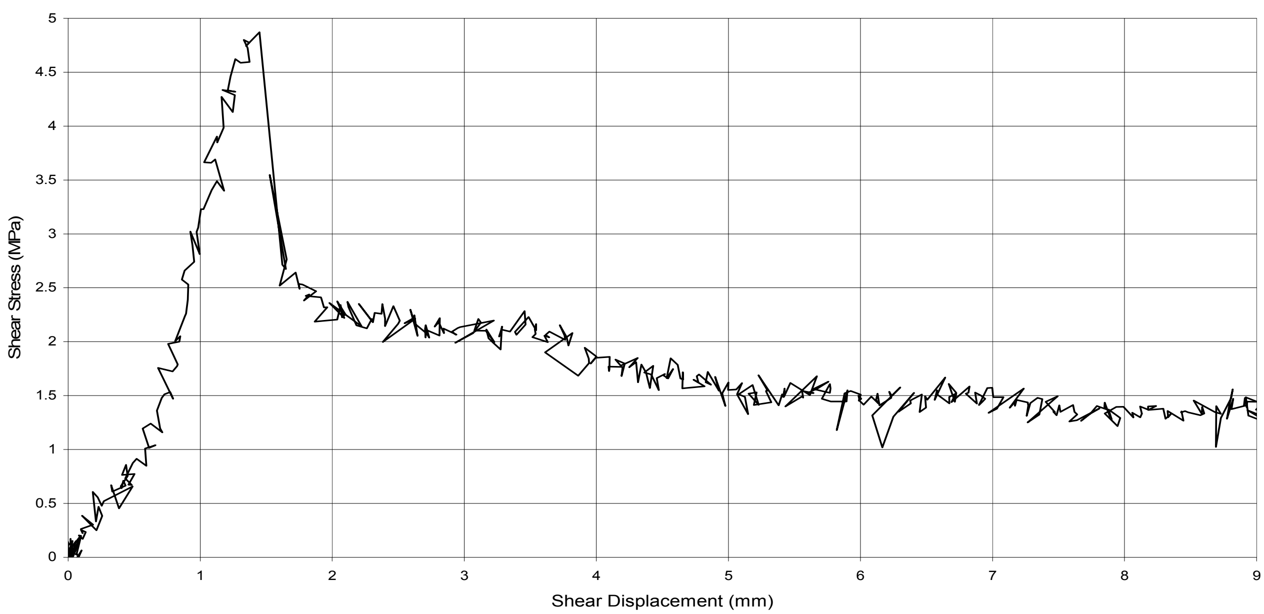

Figure F-12 DGR-5, 732.20 m

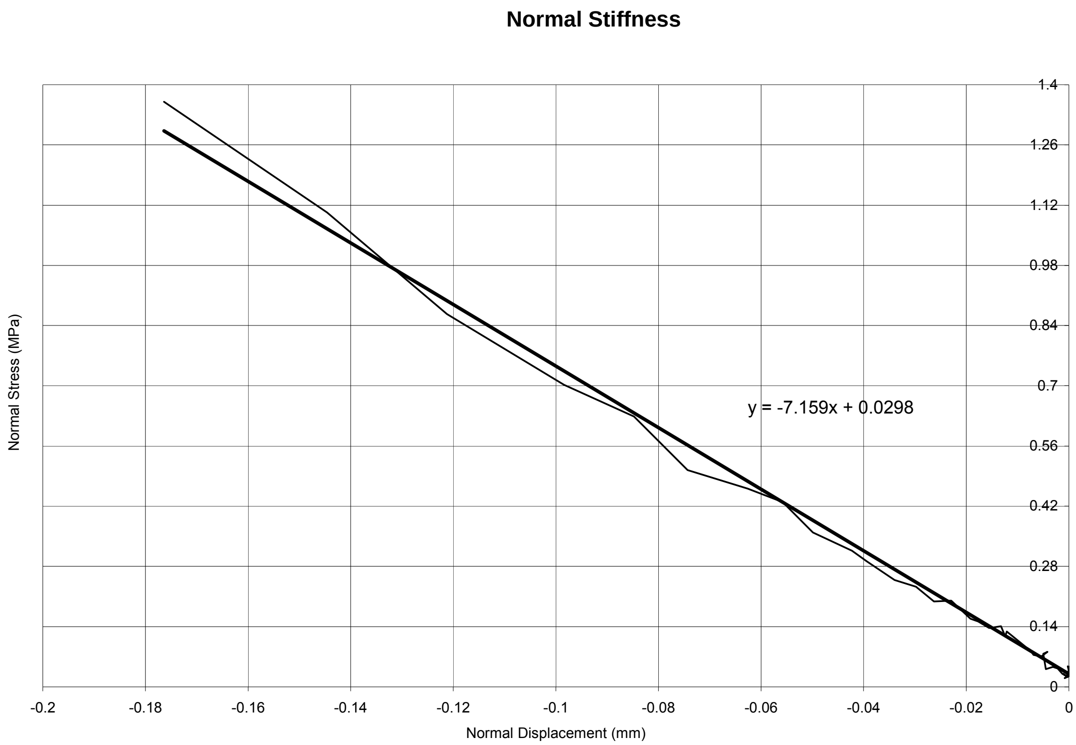

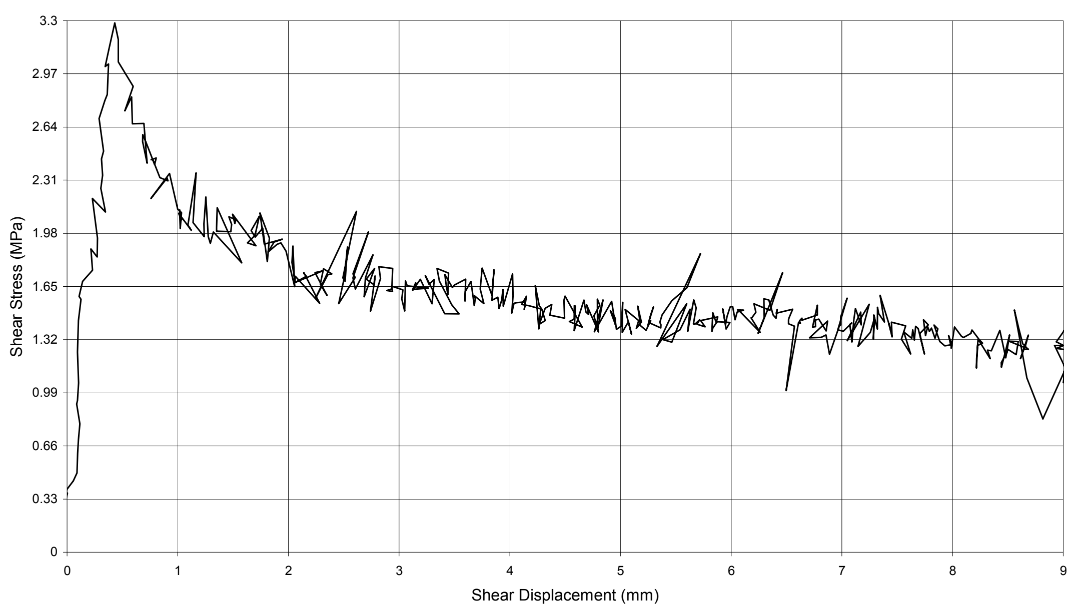

Figure F-13 DGR-5, 741.90 m

APPENDIX G

Shear Test Profiles

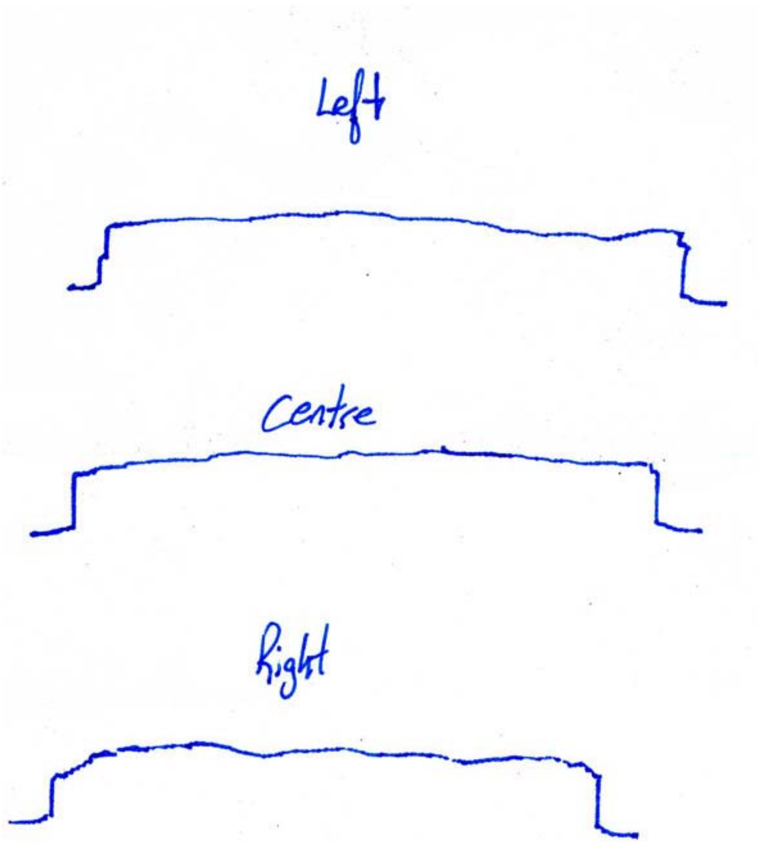

Figure G-1 DGR-2 654.00 m

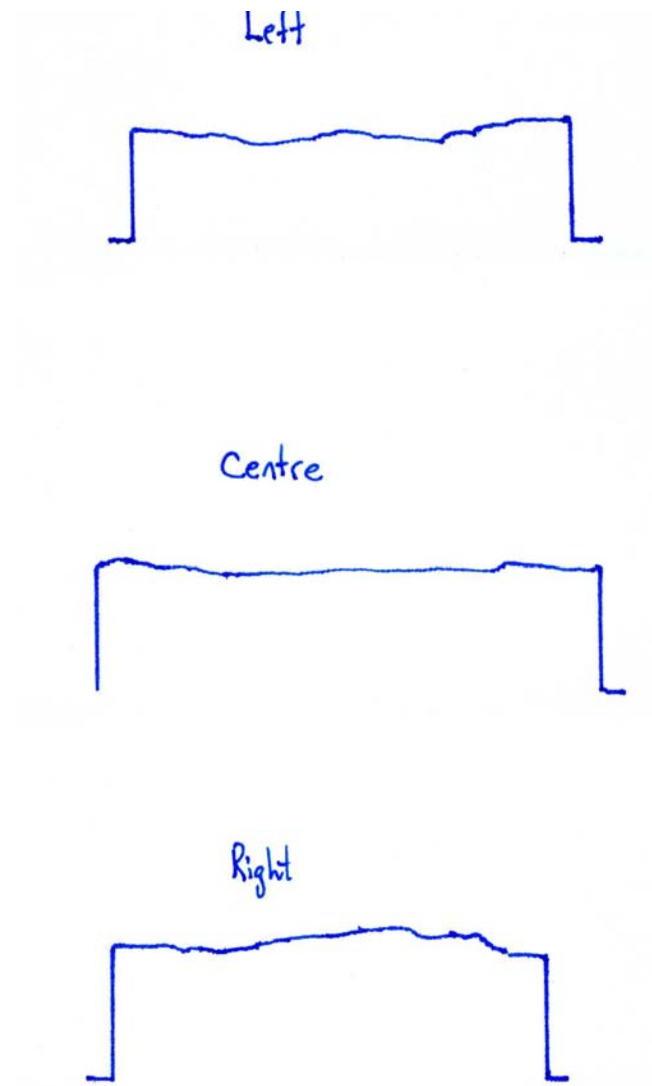

Figure G-2 DGR-2 661.36 m

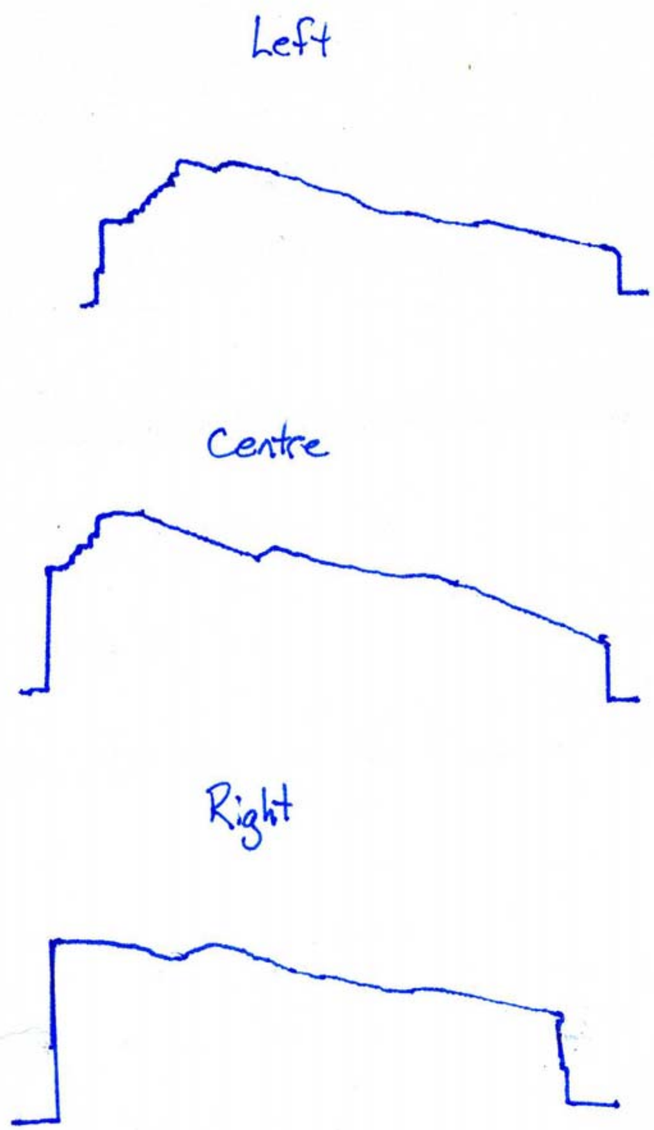

Figure G-3 DGR-2 665.29 m

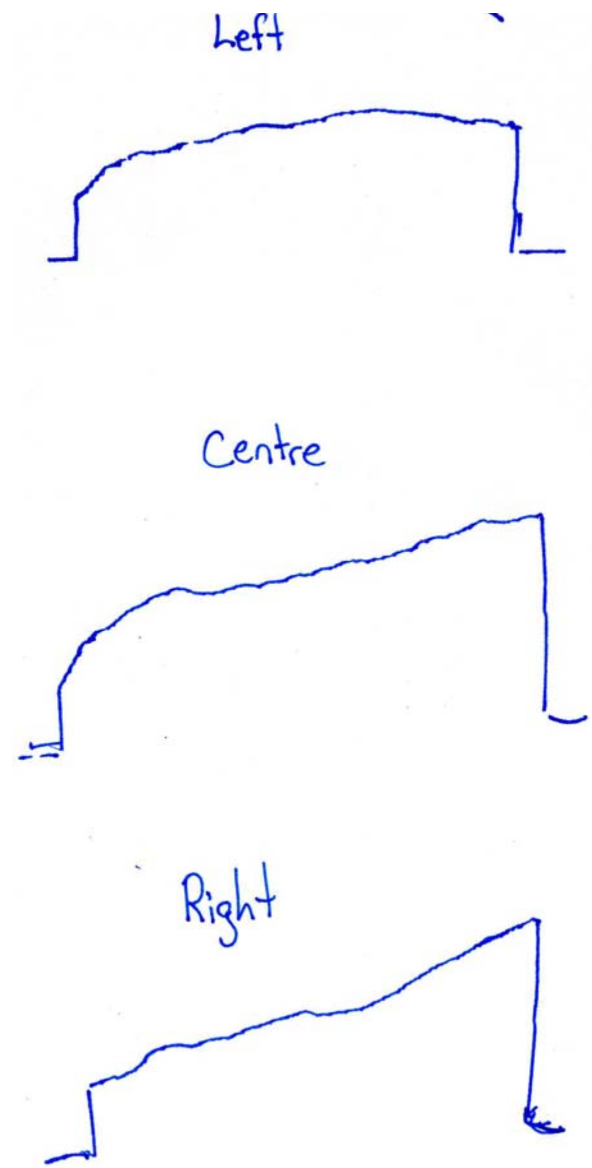

Figure G-4 DGR-3 666.10 m

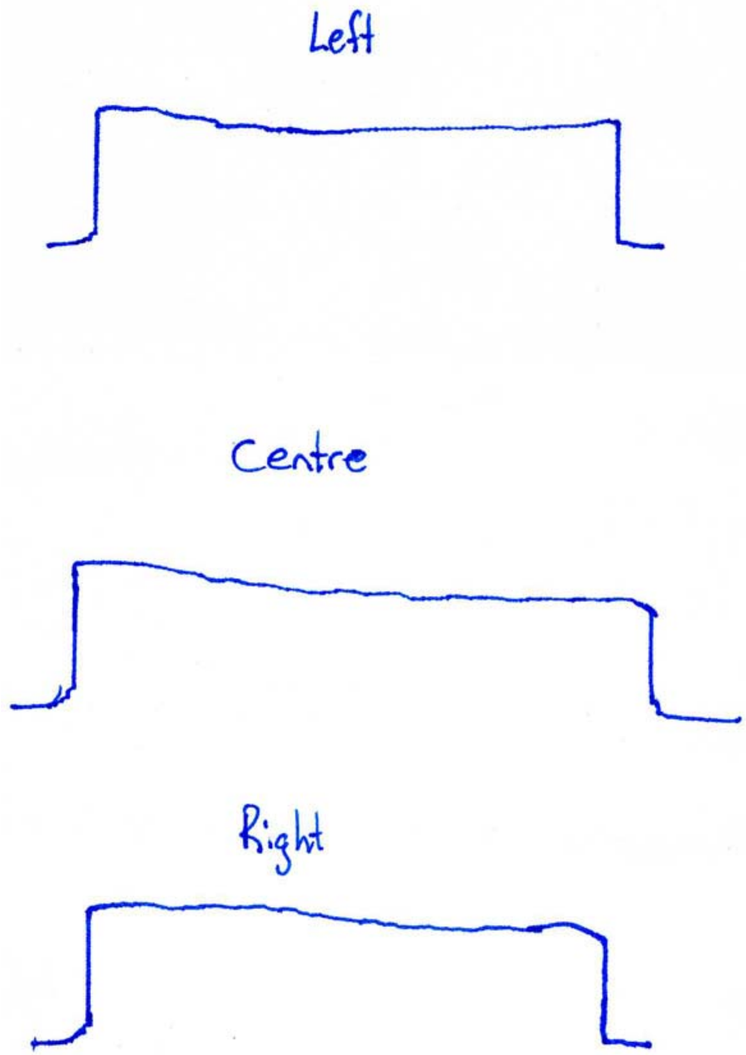

Figure G-5 DGR-4 652.93 m

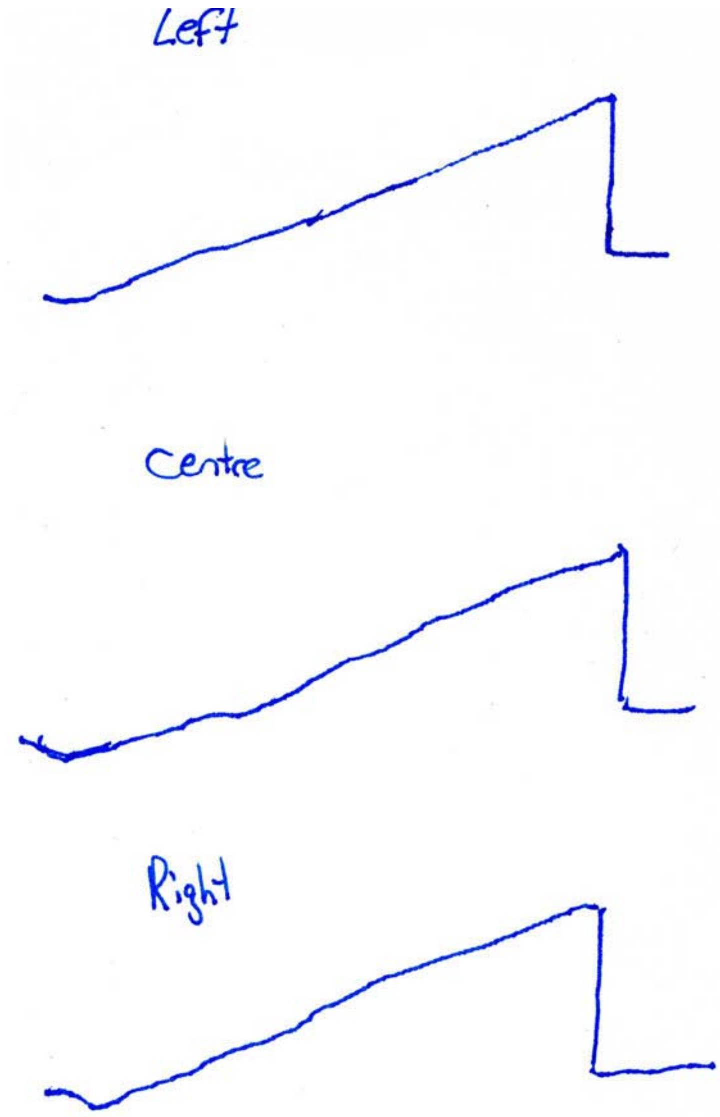

Figure G-6 DGR-4 661.90 m

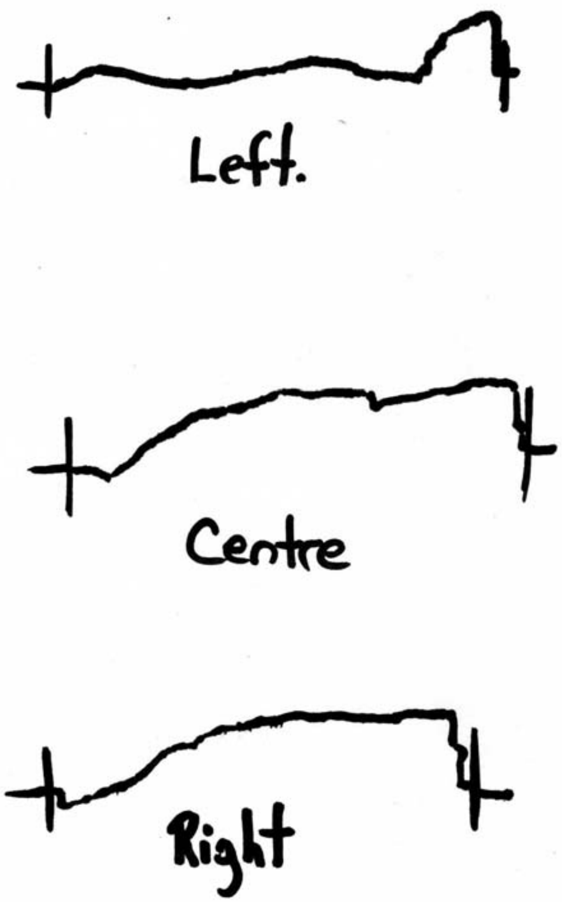

Figure G-7 DGR-5 700.70m

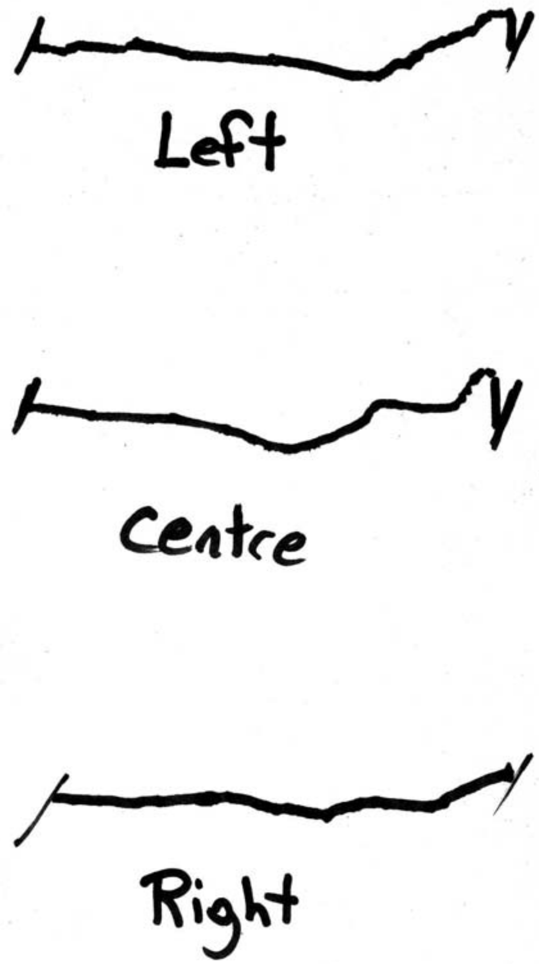

Figure G-8 DGR-5 705.90 m

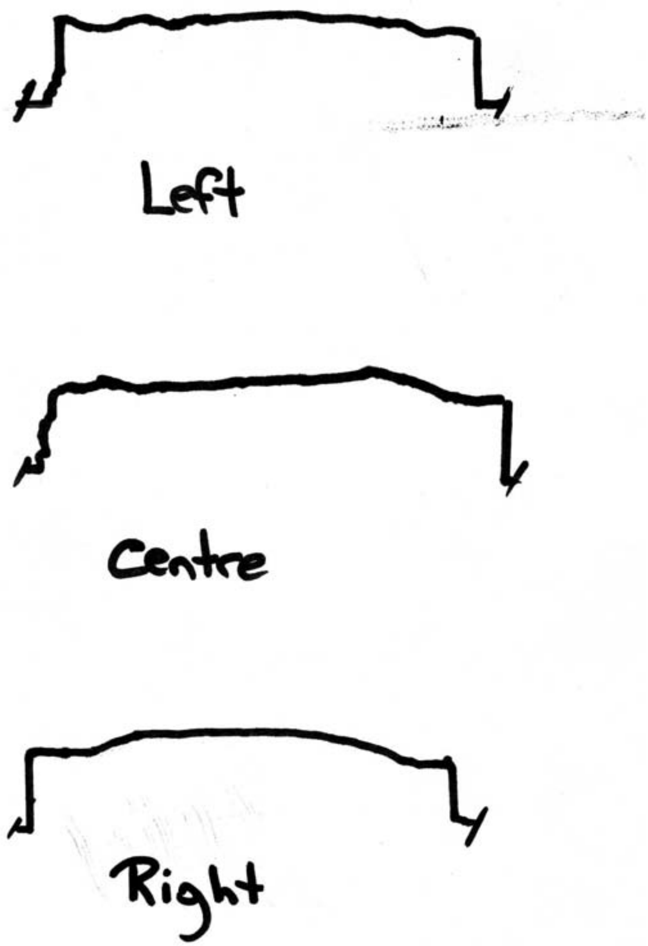

Figure G-9 DGR-5 719.65 m

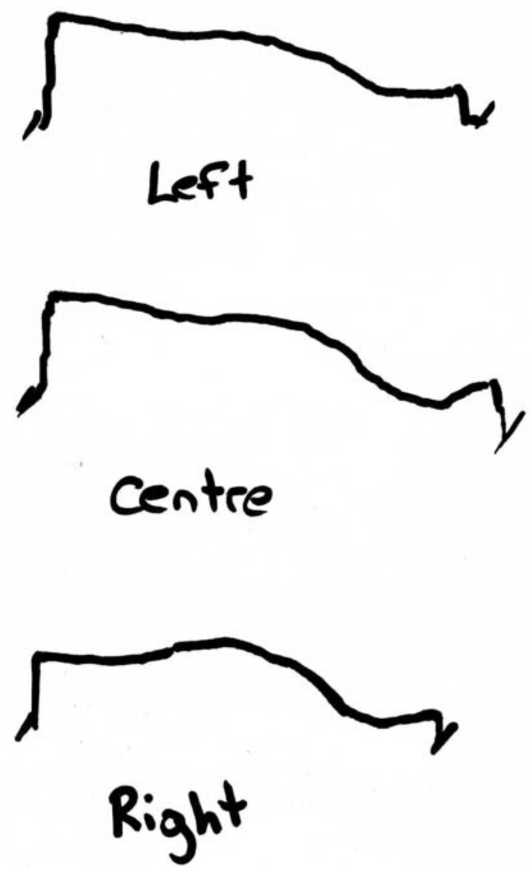

Figure G-10 DGR-5 725.50 m

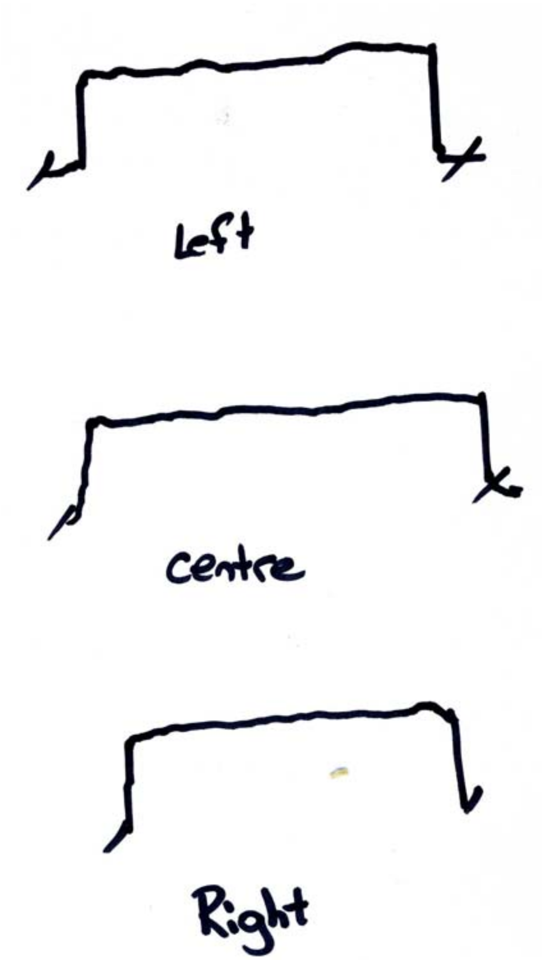

Figure G-11 DGR-5 729.70 m

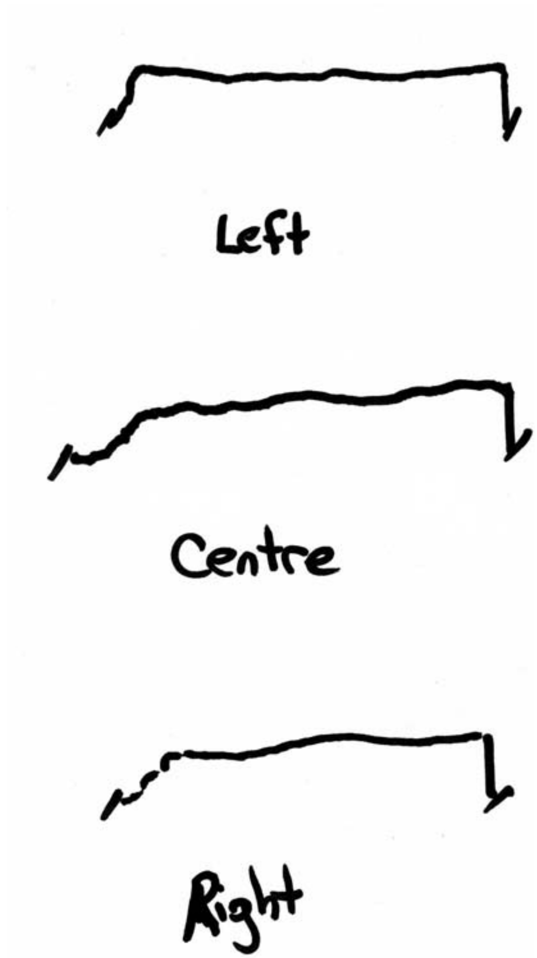

Figure G-12 DGR-5 732.20 m

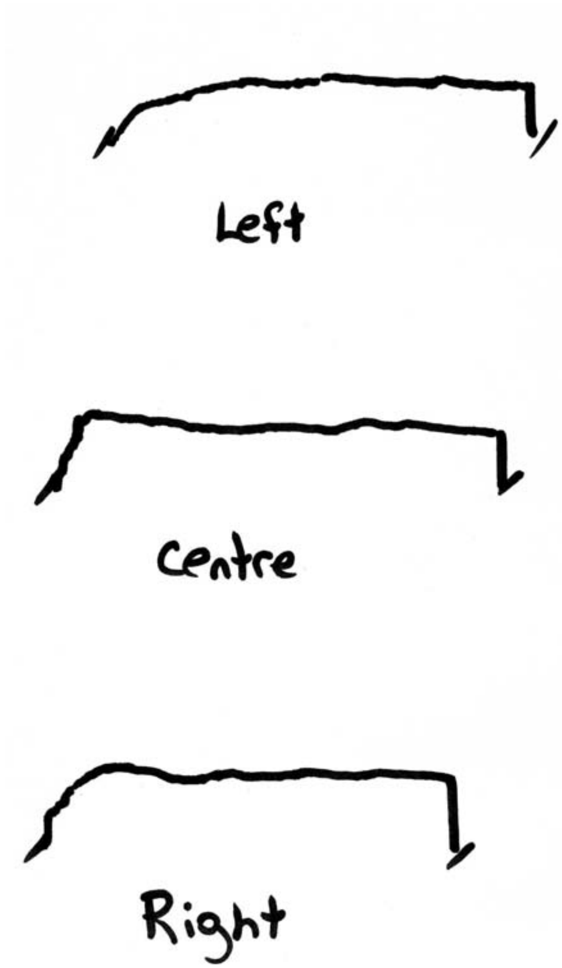

Figure G-13 DGR-5 741.90 m